PULSED FIELD ELECTROFLOTATION FOR HARVESTING MICROALGAE

A THESIS SUBMITTED TO THE GRADUATE DIVISION OF THE UNIVERSITY OF HAWAIʻI AT MĀNOA IN PARTIAL FULFILLMENT OF THE REQUIREMENTS FOR THE DEGREE OF

MASTER OF SCIENCE
IN
BIOLOGICAL ENGINEERING

MAY 2014

BY
KYLE M. KOELSCH

THESIS COMMITTEE:
DANIEL JENKINS, CHAIRPERSON
SCOTT TURN
WEI-WEN WINSTON SU

Acknowledgments

I would like to thank everyone whose efforts made this research project possible. I would like to thank my adviser Daniel Jenkins for his continual support, insight, and guidance. I would like to thank the other members of my thesis committee as well, Scott Turn and Wei-Wen Winston Su, for their guidance and valuable input. I would like to thank Susan Brown and Andrea Millan for culturing algae and supplying media for the project. I would like to thank Eunsung Kan, Vincent Cleveland, and Han Zhenlin for their technical assistance. I would like to thank Ryan Kurasaki and Charles Nelson for fabrication and machining assistance. Finally, I would like to thank Amanda Yano for her preliminary work on the real-time microalgae harvest efficiency monitoring device.

Table of Contents

Figures and Tables

List of Figures

List of Tables

1. Abstract

Microalgae are used in a number of commercial applications including biofuel production, nutraceuticals, and as feedstock for aquaculture. Typical methods for harvesting microalgae like centrifugation, microfiltration, and foam fractionation are extremely energy intensive. Reducing the energy input for harvesting microalgae would improve the overall energy balance for algae based biofuels and benefit any industry where algae is required. One method for harvesting microalgae is electrolytic flotation (electroflotation). This is simply using electrolysis-generated bubbles to float particles out of suspension and to the surface. The primary objective of this research project is to examine the effects that electrical waveform characteristics have on bubble size, gas generation efficiency, biomass separation, and lipid separation of *Chlorella* sp. from a marine media. Sets of 2^3 factorial tests were performed on a coplanar interdigitated electrode array. The waveform variables reviewed included applied potential, duty cycle, and frequency. The smallest mean bubble diameter (30.1 µm) occurred at 3V, 20%, 25 Hz. The smallest median bubble diameter (25.0 µm) occurred at 3 V, 10%, 25 Hz. The highest observed gas generation efficiency (1.69×10^{-6} (mol J^{-1})) occurred at 3 V DC. The highest observed biomass recovery (6.8%) occurred at 6 V, 20%, 25 Hz. Lipid recovery analysis was attempted as well but high variability in results rendered it inconclusive.

2. Introduction

Biofuels are being investigated as one option to decrease the United States' dependence on foreign oil and reduce greenhouse gas emissions. The Energy Independence and Security Act (EISA) requires that 36 billion gallons of renewable fuel be blended into transportation fuel by 2022 (US EPA, 2013). Microalgae are a next generation biofuel feedstock being considered to assist in meeting this mandate. Advantages of microalgae include: it can be produced domestically, some species have high oil content, and it does not compete with food crops for valuable farmland (Lam and Lee, 2012). Additionally, microalgae are a common feedstock in the nutraceutical, pharmaceutical, cosmetics, aquaculture, and chemical industries (Bishop and Zubeck, 2012).

In order to extract oils and other valuable compounds, microalgae must first be harvested from the media. This is an energy intensive process due to a number of factors including the dilute nature of the suspension (typically 0.02-0.06% total suspended solids (TSS)) (Uduman et al., 2010), the small size of the microalgae (critical dimensions 1-20 μm) (Lam and Lee, 2012), and its approximately neutral buoyancy (Griffiths et al., 2011). This small size and neutral buoyancy of microalgae coupled with its relatively high surface charge creates a relatively stable suspension that resists settling. Gravimetric sedimentation is thus not a feasible option for harvesting. This leaves filtration and screening, flocculation, centrifugation, and flotation as viable methods for separating microalgae from suspension. Many of these have significant drawbacks when it comes to the separation process (Uduman et al., 2010).

Filtering and screening equipment have limited operation times and require significant amount of maintenance. Filtration of small particles requires filters with small pore sizes which are prone to fouling. Processing large volumes of media with filtration is not practical (Uduman et al., 2010).

Flocculation can be performed with the direct addition of chemical flocculants, or by generating flocculants electrochemically with sacrificial anodes in the media. Flocculants and sacrificial anodes typically provide multi-valent metal cations which are used to reduce the zeta potential (surface charge) of the suspended algae. Eventually van der Waals forces overcome the reduced electrostatic repulsion of the net negatively charged algae and flocculation occurs followed by sedimentation (Pearsall et al., 2011; Uduman et al., 2010). The drawback with this method is that the microalgae are contaminated with undesirable metal species which have to be removed later. This method is more often used for treating waste water where the objective is to reduce turbidity. In the application of treating water, the flocculant is waste and not a desired product.

Centrifugation is a common method for harvesting microalgae. It is reliable, rapid (Christenson and Sims, 2011), able to achieve a high yield, and minimizes the water content in the desired concentrated algae sludge (Uduman et al., 2010). The draw back with this method is that it requires large amounts of energy relative to the amount of harvested microalgae (Uduman et al., 2010; Dassey and Theegala, 2013). Dassey and Theegala (2013) found that for a continuous-flow centrifuge (acceleration factor 3000 g), flow rate and percent removal were inversely related. This is intuitive because the slower flow provided more time for separation to occur. Longer residence times resulted in more energy input per volume however. For example, at a flow rate of 0.94 L min^{-1}, 94% microalgae cell removal occurred with an energy input of nearly 20 kWh m^{-3}. At a flow rate of 23 L min^{-1}, only 17% microalgae cell removal occurred but with an energy input of 0.80 kWh m^{-3}. The microalgae used in the study was *Nannochloris* sp. and was cultured to concentration of approximately 100 mg dry biomass L^{-1}.

For dilute suspensions, like those found in raceway ponds, large volumes of media need to be processed in order to get a significant yield of concentrated microalgae. Also, centrifugation is based on particle density differences in the media. In highly stable microalgae suspensions, centrifuges need to run at high rpm and increased residence times to achieve separation. These factors both contribute to the high energy input and operational costs associated with the process.

Flotation is also a potential option for removing microalgae from suspension. As bubbles rise through the flotation column, the algae adsorb to the bubbles through hydrophobic interactions and the algae are “floated” to the surface (Uduman et al., 2010; Csordas and Wang, 2004). Conventional methods of flotation consist of gas sparging and mechanical agitation. Alternative flotation methods include dissolved air flotation and electrolytic flotation. In dissolved air flotation, air is pumped into water at high pressure producing water supersaturated with air. The supersaturated water is then pumped to the flotation column where a valve is used to release the pressure. Once the pressure has been released, the dissolved gas rapidly nucleates to form bubbles. Finally, electrolytic flotation (electroflotation) simply uses electrolysis generated bubbles. Conventional gas sparging and mechanical agitation methods typically produce bubbles with diameters greater than 500 µm (Sarkar et al., 2010). Dissolved air flotation and electroflotation are able to produce substantial quantities of bubbles with diameters less than 100 µm (Sarkar et al., 2010).

In flotation, bubble size is a critical factor for efficiently separating fine (less than 20 µm) particles from suspension (Miettinen et al., 2010). Low recoveries of fine particles from suspension are primarily due to the low number of bubble-particle collisions occurring (Miettinen et al., 2010). Increasing the number of smaller bubbles per volume of generated gas will increase the overall surface area of the gas-liquid interface and thus increase the probability that a bubble-particle collision will occur. Higher rates of bubble-particle collisions lead to higher flotation rates of the particles out of suspension (Khosla et al., 1991; Miettinen et al., 2010). When considering the energy efficiency of a flotation method, it is important to not only look at the energy input per volume of gas generated, but also the separation effectiveness of the bubbles.

3. Objectives

Objectives of the proposed research include:

1. Design, fabricate, and operate a benchtop scale electroflotation assembly.
2. Conduct experiments in a 2^3 factorial experimental design to investigate the effects that the applied potential, the duty cycle, and the frequency have on bubble size, gas generation efficiency, biomass separation, and lipid separation on *Chlorella* sp. from a marine media.

4. Background and Literature Review

The following will discuss and compare electroflotation to gas sparging and dissolved air flotation as well as review pulsed electrolysis in greater detail. Analytical methods to evaluate flotation methods are discussed at the end of the section.

4.1. Flotation: Thermodynamic Comparison

Gas sparging, dissolved air flotation, and electroflotation all use bubbles to remove particles from suspension. An energy analysis of input energy to volume of gas supplied shows that electroflotation is by far the most energy intensive method to generate a given volume of bubbles. The thermodynamic energy cost of electrolytically generated gas can be calculated by multiplying the applied potential in volts, E_p ($J\ C^{-1}$), and Faraday's constant, F, 96485 ($C\ mol[e^-]^{-1}$), to yield energy in terms of joules per moles of electrons. Finally, multiplying this value with the stoichiometric ratio of moles of electrons required to generate one mol of gas, ratio α, provides the energy required for the production of gas on a molar basis E_v ($J\ mol[gas]^{-1}$).

$$E_v \left|\frac{J}{mol\ [gas]}\right| = E_p \left|\frac{J}{C}\right| \cdot F \left|\frac{C}{mol\ [e^-]}\right| \cdot \alpha \left|\frac{mol\ [e^-]}{mol\ [gas]}\right| \qquad (1)$$

The ratio α can be estimated experimentally by relating the mean observed current to steady state gas generation rate. The exact value of α depends on the exact half reactions and gases generated at the respective electrodes. Below are the half reactions for freshwater and seawater electrolysis as well as the Nernstian redox potentials. For freshwater electrolyis, the half reactions are:

Reaction at the Cathode:

$$4H^+ + 4e^- \rightarrow 2H_{2(g)} \tag{2}$$

Reaction at the Anode:

$$2H_2O_{(l)} \rightarrow 4e^- + 4H^+ + O_{2(g)} \tag{3}$$

Overall Reaction:

$$2H_2O_{(l)} \rightarrow 2H_{2(g)} + O_{2(g)} \quad \Delta E_{rxn} = -1.23\ V \tag{4}$$

For seawater electrolysis (599 mM NaCl), the predominating half reactions are:

Reaction at the Cathode:

$$2H_2O_{(l)} + 2e^- \rightarrow 2OH^- + 2H_{2(g)} \tag{5}$$

Reaction at the Anode:

$$2Cl^- \rightarrow 2e^- + Cl_{2(g)} \tag{6}$$

Overall Reaction:

$$2H_2O_{(l)} + 2Cl^- \rightarrow Cl_{2(g)} + 2OH^- + H_{2(g)} \quad \Delta E_{rxn} = -1.79\ V \tag{7}$$

In fresh water, molecular oxygen (O_2) is the primary oxidation product at the anode, but in seawater rates of molecular chlorine (Cl_2) generation can be significantly higher (Balaji et al., 2009).

Assuming formation of only O_2 at the anode (fresh water), α=4/3 (4 e^-/ (2 $H_{2(g)}$ + 1 $O_{2(g)}$))

Assuming formation of only Cl_2 at the anode (seawater), α=2/2 (2 e^-/ (1 $H_{2(g)}$ + 1 $Cl_{2(g)}$))

Assuming 100% thermodynamic efficiency:

Fresh water, substituting α=4/3 and E_p=1.23 V into equation 1 ⟶ E_v =158.2 kJ mol[gas]$^{-1}$

Seawater, substituting α=2/2 and E_p=1.79 V into equation 1 ⟶ E_v = 172.7 kJ mol[gas]$^{-1}$

In contrast to electroflotation where gas generation requires electrochemical energy to molecularly transform components in solution, gas sparging and dissolved air flotation require energy to compress gas. Compression requires gas molecules to be confined to a smaller volume (higher concentration).

Starting with the fundamental property relation (Koretsky, 2004):

$$dg = -sdT + vdP \tag{8}$$

Where g is molar Gibbs energy, s is molar entropy, T is temperature, v is molar volume, and P is pressure. Holding temperature constant, equation 8 becomes:

$$dg = vdP \tag{9}$$

Integrating both sides of equation 9:

$$g(P_2) - g(P_1) = \int_{P_1}^{P_2} vdP \tag{10}$$

Substituting molar volume with its equivalent expression from the ideal gas law, the chemical/ thermodynamic energy required for compression can be estimated as the equation:

$$g(P_2) - g(P_1) = \int_{P_1}^{P_2} \frac{RT}{P} dP \tag{11}$$

Completing the integration on the right side of equation 11:

$$g(P_2) - g(P_1) = RT\ln\left(\frac{P_2}{P_1}\right) \tag{12}$$

Leading to the final equation:

$$\text{Energy}\left|\frac{J}{mol[gas]}\right| = RT\ln\frac{p_f}{p_i} \tag{13}$$

Where R is 8.3145 (J mol^{-1} K^{-1}), T is temperature in K, p_f is final pressure and p_i is ambient (initial) pressure in absolute terms.

For a brief comparison of flotation methods, one sparging source and one dissolved air flotation source were selected. For the foam fractionation assembly of Csordas and Wang (2004), gas was provided at 54.7 psi absolute pressure, taking the ambient pressure to be 14.7 psi absolute and standard temperature (298 K), the resulting thermodynamic energy cost is 3.3 kJ $mol[gas]^{-1}$. For the dissolved air flotation assembly of Henderson et al. (2008) gas was pressurized to 551.3 kPa absolute, taking the ambient pressure to be 101.325 kPa and standard temperature (298 K), the resulting thermodynamic energy cost is 4.2 kJ mol[gas]$^{-1}$.

Clearly, on a thermodynamic basis, gas sparging and dissolved air flotation are the more energy efficient methods to deliver gas to a media. To be competitive, electrolytically generated bubbles must provide significant advantages with respect to speed (grams of algae removed per second) and efficiency (grams of algae removed per joule) of separation of algae from suspension.

4.2. Bubble Size

As previously mentioned, bubble size has a significant effect on the capacity of a given quantity of gas to remove fine particles from a suspension. It has been demonstrated that bubbles of 600 μm-1000 μm are not effective at removing particles less than 20 μm in diameter (Sarkar et al., 2011). Conventional gas sparging and mechanical agitation methods typically produce bubbles with diameters greater than 500 μm (Sarkar et al., 2010) and thus most bubbles resulting from these methods are not sufficiently small to efficiently remove these fine particles. Thus electroflotation and dissolved air flotation are theoretically more efficient on a volumetric basis for floating fine particles out of suspension.

4.3. Electrolysis and Bubble Size

Bubble generation during electrolysis can be described in three sequential steps: nucleation, growth, and detachment (Khosla et al., 1991). As a reduction or oxidation reaction proceeds, the environment around the electrode becomes saturated with gas (Khosla et al., 1991). Once a critical supersaturation level is reached, bubbles begin to nucleate on the surface of the electrode (Khosla et al., 1991). The bubbles continue to grow as saturated gas diffuses into the bubbles (Khosla et al., 1991). Detachment occurs once the buoyant force overcomes the adhesion force between the bubble and the electrode surface or a shearing force rips the bubble into the bulk electrolyte (Khosla et al., 1991). Depending on the spatial distribution of saturated gas near the electrode surface, the bubble may continue to grow after detachment. Sarkar et al. (2010) reported an 8x increase in hydrogen bubble volume within the first few millimeters after detachment from the electrode surface.

The factors that affect the size of electrolytically generated bubbles are both physical and chemical. Electrode morphology and geometry are physical factors that will have a significant influence on bubble size (Khosla et al., 1991; Sarkar et al. 2011). For example, wires with thinner diameters produce smaller bubbles than thicker diameter wires (Khosla et al., 1991; Sarkar at al., 2011; Sarkar et al., 2010). Cell agitation through stirring, shaking, or application of a shear flow is another physical factor to consider. pH is an important chemical factor with an acidic medium leading to an increased hydrogen bubble size and a decreased oxygen bubble size (Sarkar et al., 2010). The composition of the electrode and its position in the electromotive series (oxidation potential) will also affect bubble sizes (Sarkar et al., 2010). Finally, current pulsing has been demonstrated to produce smaller bubbles than constant direct current (DC) (Khosla et al., 1991).

4.3.1. Pulsed Field Electrolysis

As opposed to constant DC electrolysis, pulsed field electrolysis has rapid breaks in the current. Pulsed current is achieved by pulsing the applied potential.

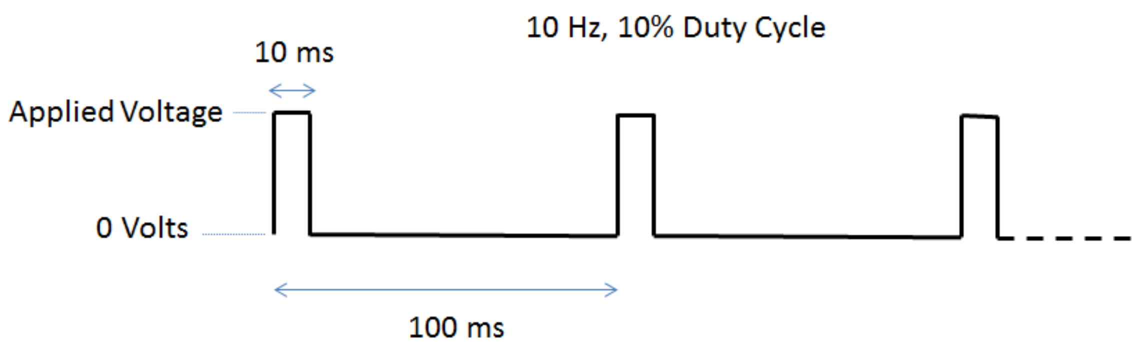

Figure 1. Diagram of 10 Hz, 10% Duty Cycle Pulse Cycle

Current pulses can be beneficial in the efficiency of fine particle flotation because they promote an improved bubble flux and also a reduction in bubble size (Khosla et al., 1991).

Bubble flux is the number of bubbles distributed over a given area and is determined by the number of nucleation sites. Periodic disruption of current (i.e. pulsed current) enables diffusion of redox reactants more uniformly across the electrode surface diminishing high current density areas (Chandrasekar and Pushpavanam, 2008). High current density areas like edges and defects on electrode surfaces form nucleation sites and are not conducive to homogenous nucleation and bubble flux (Khosla et al., 1991). A uniform distribution of bubbles generated across the electrode surface will increase the areas in the electroflotation cell where bubble particle-collisions are occurring. Evenly distributed rising bubbles will simply have a more net like effect and capture more particles on their way to the surface.

Bubble size reduction due to current pulsing is a function of the increased opportunity for detachment (Khosla et al., 1991). If electrolysis occurs continuously, bubbles can grow significantly while they are in the process of detaching from the electrode surface. By periodically interrupting the current, bubbles' growth rates are diminished with the result that proportionally more bubbles will be closer to the minimum size required for detachment. It is worth noting that the effect of current pulses on bubble size appears to be a novel research area and that there is very little available literature about the topic.

4.3.2. Coplanar, Interdigitated Electrode Array Design

A coplanar, interdigitated electrode array design has several efficiency advantages over a parallel plate design. Interdigitating the electrodes allows for much smaller electrode spacing which reduces the internal resistance of the electrolysis cell. In a parallel plate system, there are significant constraints on the spacing between anode and cathode. Eventually gas pockets between the electrodes will begin to form and cell resistance will rise (Nagai et al., 2003). The coplanar, interdigitated design avoids this situation because the bubbles form only at the upward facing surface of the electrodes. This orientation also is less susceptible to bubble coalescence. As bubbles detach from the electrodes in a parallel plate electrolysis cell, they encounter and merge with other bubbles forming at the electrode’s surface. A coplanar orientation does not present the opportunity for bubbles to move across the electrode surface and coalesce. The final advantage the coplanar interdigitated design has over the parallel plate design is that it distributes bubbles more evenly throughout the volume of the electrolysis cell. Bubbles will be detaching across the entire electrode array floor of the cell rather than just the walls and thus more effectively sweep algae out of suspension.

4.4. Reactive Chlorine Generation During Marine Electrolysis

Marine electrolysis produces chlorine gas and a portion of this gas may react in the media to produce hypochlorite (ClO^-) and other reactive chlorine species (Belmont et al., 1998; Gao et al., 2010). Chlorine gas in the bulk reacts with the water to form ClO^- in the following reaction mechanism (Belmont et al., 1998).

At anode: $$2Cl^- \rightarrow 2e^- + Cl_{2(g)} \tag{14}$$

In Bulk: $$Cl_{2(g)} + 2H_2O_{(l)} \leftrightarrow HClO_{(l)} + Cl^- + H_3O^+ \tag{15}$$

$$HClO_{(l)} + H_2O_{(l)} \leftrightarrow ClO^- + H_3O^+ \tag{16}$$

Hypochlorite is an oxidizer and could potentially oxidize the algae cells. For example, Gao et al. (2010) demonstrated that algae exposed to electrochemically generated reactive chlorine species (chlorine, hypochlorous acid HClO, and hypochlorite ClO^-) and an electric field could have their cell walls damaged and ruptured. This compromise in cellular integrity was followed by oxidation of components inside the cell such as chlorophyll (Gao et al., 2010). In order to mitigate degradation effects on algae,

algae recovery needs to be possible with relatively little gas generation and relatively little reactive chlorine generation.

4.5. Analytical Methods

The following sections review different approaches for analysis of bubble generation and flotation as a method of separating materials from suspension.

4.5.1. Bubble Sizing Approaches

Multiple options were considered for bubble sizing. Doppler acoustics can be used to determine the velocity of bubbles (Didenkulov et al., 2000). For rising bubbles, size can be estimated based on terminal velocity. Light scattering (Dehaeck and van Beeck, 2008), acoustics (Zhang et al., 2012), and optical methods (Khosla et al., 1991) are other potential options for bubble sizing.

A substantial amount of time was spent attempting to size bubbles through acoustic measurements, so this will be discussed in greater detail. Bubbles upon detachment or following an impulsive force, oscillate with a characteristic resonance frequency which is related to the size of the bubble. This size dependent oscillation is designated as "Minnaert resonance," and is defined mathematically as (Zhang et al., 2012).

$$f_o = \frac{1}{2\pi R_o}\sqrt{\frac{3\kappa P_o}{\rho_l}} \qquad (17)$$

where f_o is fundamental (Minnaert) resonant frequency, R_o is the bubble radius, κ is the polytropic index, P_o is the absolute liquid pressure, ρ_l is the liquid density.

4.5.2. Experimental Levels

Experimental levels for frequency and duty cycle were chosen based on a review of the literature. Also, intuitively, if frequency and duty cycle were too high, the current interruptions would not be sufficiently long for bubble detachment or for significant diffusion to replenish depleted reactants near the electrode surface. For example, Khosla et al. (1991) used a frequency of 33 Hz and duty cycles of 100%, 50%, 25%, 20%, 5%. Their results demonstrated that lower duty cycles were more effective at generating smaller bubbles. These testing parameters provided reference levels around which the experimental levels of 25 Hz and 100 Hz with 10% and 20% duty cycles were selected for this investigation.

4.5.3. Lipid Quantification with Nile Red

Quantifying lipid content in algae is of great importance in identifying strains and growing conditions to be optimized for biofuel production. Analyzing lipid contents in samples traditionally involves a solvent extraction of the lipids followed by gravimetric or spectrophotometric analysis (Bertozzini et al., 2011). These methods are time intensive and not suitable where high-throughput is required (Bertozzini et al., 2011; Feng et al., 2013). Experimental errors from these analyses may also occur due to failure to recover or convert 100% of the analyte in each of the numerous processing steps involved (extraction, saponification, etc.) (Bertozzini et al., 2011).

An effective alternative is the lipid selective fluorescent probe Nile red (9-diethylamino-5H-benzo[α]phenoxa-phenoxazine-5-one) (Bertozzini et al., 2011). It is photostable and intensely fluorescent in the presence of organic solvents and hydrophobic materials (Bertozzini et al., 2011). Peak fluorescence emission generally occurs within the range from 580 nm (Feng et al., 2013) to 600 nm (Bertozzini et al., 2011) in the presence of lipids. Nile red can be used in-vivo for quantification of lipid content in algae (Bertozzini et al., 2011). The intensity of the fluorescence is a function of the lipid content in the media. Because Nile red can be used in-vivo (Feng et al., 2013) and it is highly fluorescent, it can be quite suitable for analyzing small samples at high throughput. This is particularly advantageous in lab-scale multifactorial experiments and that is why it was selected to analyze the lipid contents of collected samples.

5. Materials and Methods

As mentioned previously, the bubble size distribution will have a direct influence over the effectiveness of floating small particles out of suspension. It is desired to have a large number of smaller bubbles per mol of gas generated. However, this consideration needs to be balanced with the need for high gas generation rates to achieve rapid separation on an industrial scale. Even if the bubbles are smaller, there may be too few of them to achieve any significant separation in a practical amount of time. Therefore an additional and complementary investigation is necessary where the flotation of particles, in this case microalgae, from suspension is observed. Gas generation rate efficiency is another parameter of interest as it is desirable to use the least amount of energy to generate gas. Finally, lipids are a valuable component in algae. Examining lipid separation would not be necessary if all the lipids were contained within the algae. The algae separation analysis via photometric methods would be a sufficient indicator of lipid separation. It was discovered however that high rates of cell lysis were likely occurring during electrolysis in a marine environment, and that recovery of the lipid fraction might be worth investigating separately (i.e. electroflotation might be valuable as a single step process for lipid recovery from media). Cell lysis is reviewed in more depth in section 6.4.3. The following sections discuss the approach followed to examine the effects that changing the electrical waveform has on bubble size, gas generation efficiency, biomass separation, and lipid separation.

5.1. Electrode Array

For controlled comparisons of the experimental treatments in this study, it was critical that the electrode array was physically and chemically stable during the conditions of the tests. To address this concern, dimensionally stable anode (DSA) materials were used in the fabrication of the electrode array. DSA electrodes are also known as mixed metal oxide (MMO) anodes and usually consist of titanium thinly coated with a mixture of metal oxides such as ruthenium oxide (RuO_2) (Fathollahi et al., 2011; Zhou et al., 2011), iridium oxide (IrO_2) (Fathollahi et al., 2011; Zhou et al., 2011), titanium oxide (TiO_2) (Fathollahi et al., 2011), and tantalum oxide (Ta_2O_5) (Zhou et al., 2011). DSA electrode coatings may contain any combination of these components in various amounts but RuO_2 and/or IrO_2 are generally in the coating. The metal oxide coating of DSA electrodes are special in that they are conductive (Fathollahi et al., 2011) and provide excellent resistance to passivation and corrosion. For SEM images of the electrodes used in the fabricated array, see Appendix 1. Our electrode MMO coating consisted of titanium ribbon coated with IrO_2/Ta_2O_5 (IrO_2/Ta_2O_5 MMO Titanium Ribbon Anode, Suzhou Fenggang Titanium Products and Equipment Manufacturing Co., Suzhou, China). The electrode array was a coplanar, interdigitated design made up of layers of electrode ribbon. The result is a “sandwich” layout that alternates between anode and cathode with insulation in between (Figures 2 and 3).

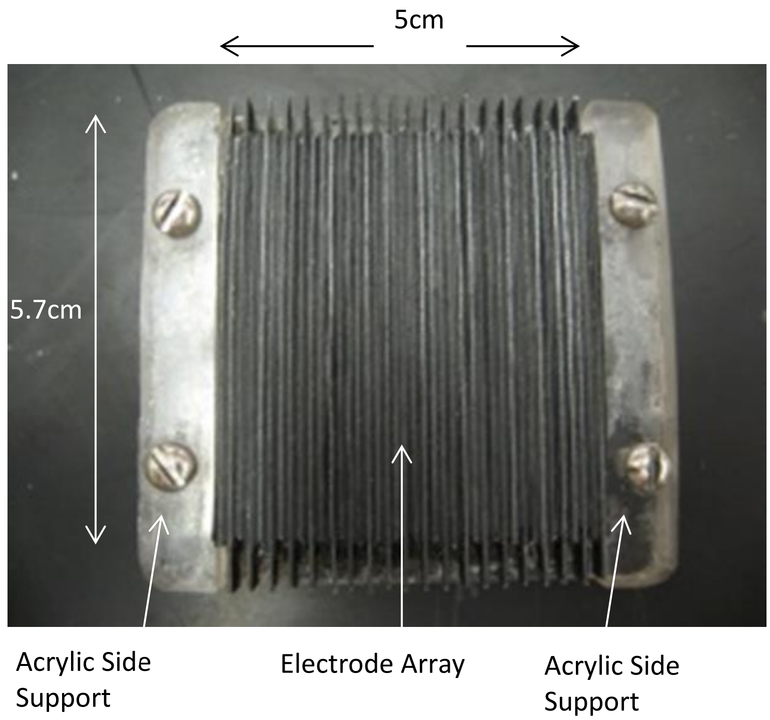

Figure 2. Top View of Fabricated Electrode Array

5.1.1. Electrode Array Fabrication

As previously mentioned, the electrode array consisted of layers of DSA ribbon. The ribbon pieces were 0.57 mm thick, 6.15 mm tall, and were cut to 5.7 cm length. Each piece was insulated from its neighbor by layering strips of electrical tape to a thickness of 0.7 mm. The individual ribbon pieces were interdigitated and alternated anode and cathode throughout the array (Figure 3). After a 5 cm stack of array was prepared, the pieces were clamped together and the bottom of the array was glued to an acrylic base. Acrylic side supports were then added to compress the array together and prevent vertical intrusion of media into the array (Figure 2).

All the anodic digits were connected to a common electrical bus, and similarly all the cathodic digits were connected to a different bus. This was not a simple task due to inability to solder to the DSA ribbon's titanium core and the small spacing between digits. To establish electrical contact, graphite interconnects were wedged between each of the nearest DSA ribbons on the same electrical bus (Figure 3).

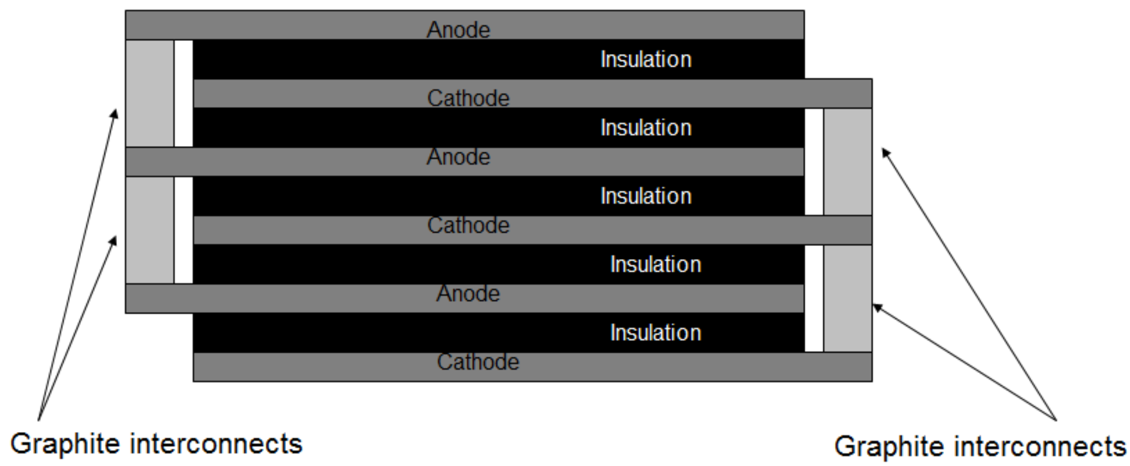

Figure 3. Portion of Electrode Array Diagram

Graphite was selected because it was highly conductive and easy to machine into the desired shape. Every interconnect had to be hand sanded to achieve the best fit possible between digits in order to ensure good connectivity. Three wire connections for each bus of the array were also incorporated. See Appendix 2 for the wire connection picture and resistances in the electrical bus.

5.2. Bubble Column Fabrication

The bubble column was constructed with 5.7 mm thick clear acrylic sheet. The inner dimensions were 4.1 x 3.9 x 14.4 cm (230.3 mL). The feed entered through a centered port 10 cm from the bottom and the treated flow exited through a centered port 2 cm above the bottom of the vessel. The bubble column was sealed to the electrode array by epoxy (PermaPoxy 5 Minute General Purpose Epoxy, Permatex, Hartford, CT) to create the electroflotation cell (Figure 4).

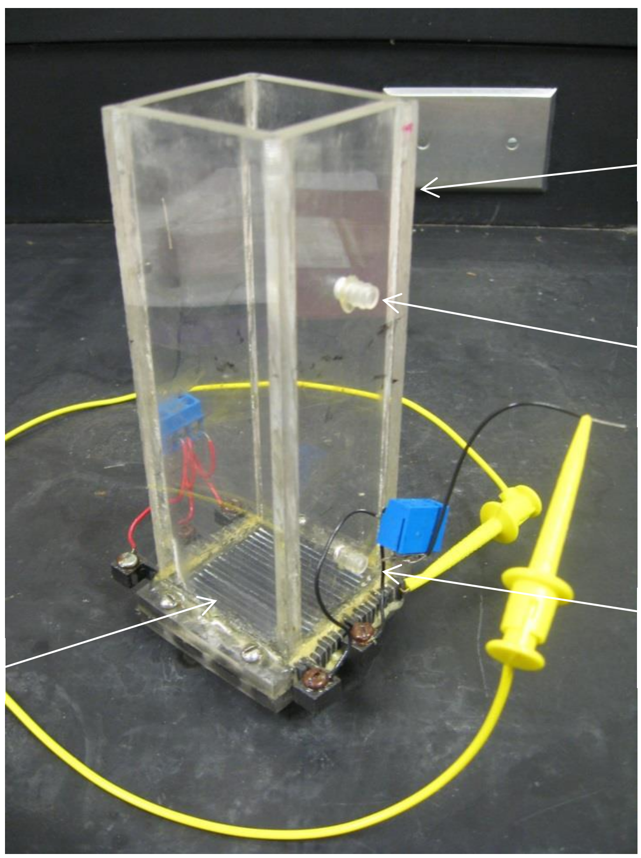

Figure 4. Electroflotation Cell Picture. The yellow mini hook cable was required to replace a broken wire connection.

5.3. Signal Generation

Applied potential (V), duty cycle (%), and frequency (Hz), were the variables investigated in the research project. Applied potential was set on a digital triple output power supply (E3631A, Agilent Technologies, Santa Clara, CA) and frequency and duty cycle were controlled by an Arduino microcontroller (Uno, Arduino, Torino, Italy) switching current through an n-channel power MOSFET (Metal-Oxide Semiconductor Field-Effect Transistor; IRF 3703, International Rectifier, El Segundo, CA) (Figure 5).

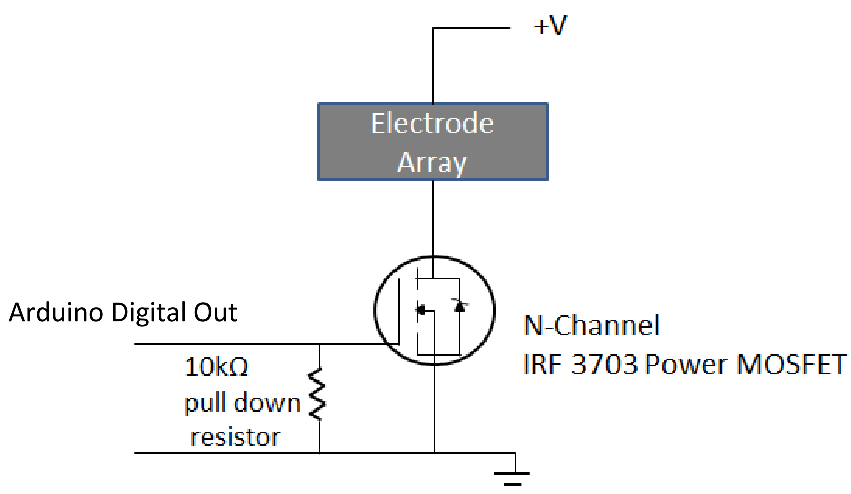

Figure 5. MOSFET Circuit for Switching Current Through the Electrode Array

5.4. Real-time Microalgae Harvest Efficiency Monitoring

To monitor harvesting efficiency in real-time in a flow-through configuration, algae flowing through the electrolysis cell were also directed through two customized optical cells. The setup was configured to estimate the optical density of the influent stream, as well as the difference in optical densities of the influent and treated streams, based on first principles. In addition, the custom configuration enabled automatic correction for biofilm effects on the optical cells. Optical densities were used as a proxy for suspended solids content, such that removal efficiency could directly be inferred from the observed data. By definition, absorbance A is equivalent to the logarithmic ratio of light intensity I_o incident to an optical path to the intensity I transmitted through it (Bui and Hauser, 2013).

$$\mathrm{A} = \log\frac{\mathrm{I_o}}{\mathrm{I}} \tag{18}$$

By the Beer-Lambert Law (Bui and Hauser, 2013), absorbance is also related to the concentration of optically absorbent material in the path:

$$\mathrm{A} = \varepsilon \mathrm{lc} \tag{19}$$

Where ε is the extinction coefficient ($cm^2\ mol^{-1}$) of the material, l is the pathlength (cm), and c is concentration ($mol\ cm^{-3}$).

Each of the optical cells consisted of a pair of 650 nm laser diodes illuminating a set of corresponding photodiodes (Figure 6).

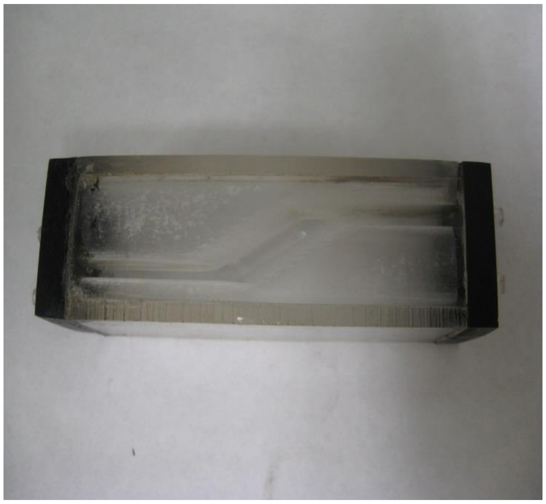

(a)

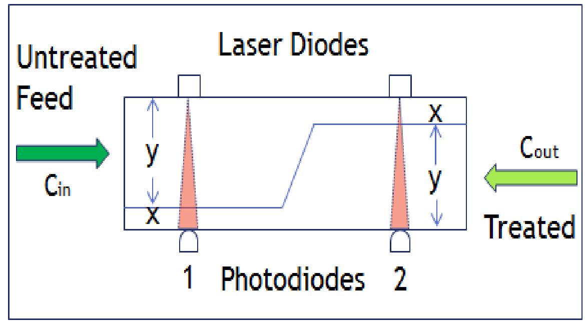

(b)

Figure 6. Fabricated Optical Cell for Measuring Algae Optical Properties (a). Two sets of laser diodes and photodiodes are configured to measure optical density of the two unique light paths across the cell (b).

The 650 nm laser diodes were selected because they are near the absorbance peak of chlorophyll. Optical cells were constructed so that the respective light paths travel different distances through two different media being analyzed. If the laser intensities were held constant, these different path lengths would lead to different light intensities experienced by the corresponding photodiodes thus resulting in different photocurrents. In our system however, the intensity of one of the lasers (laser 2) is regulated by a custom circuit such that the photocurrents are identical (Figure 7).

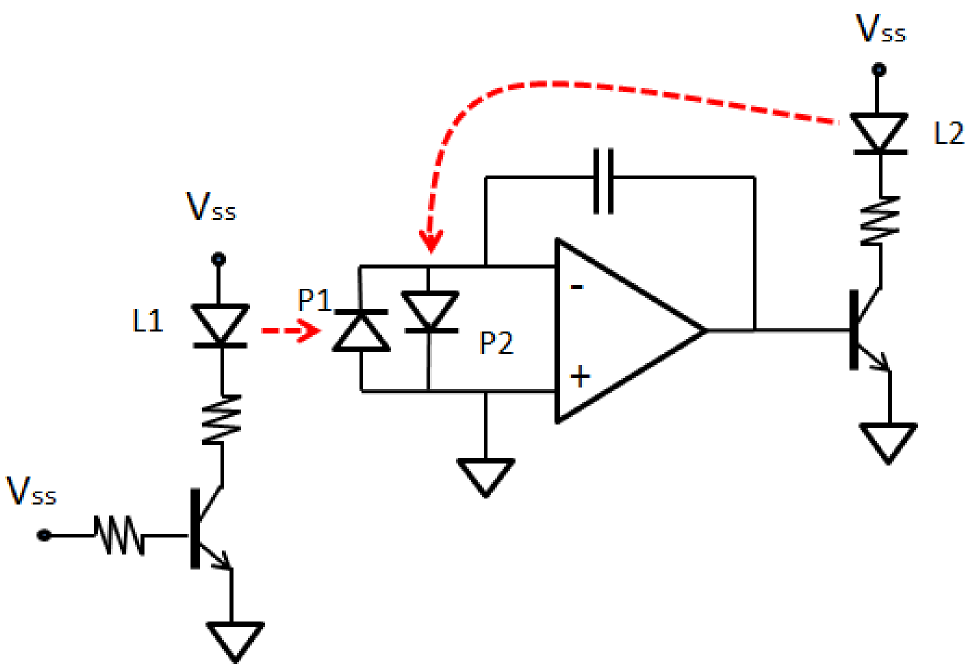

Figure 7. Photometric Feedback Circuit. The intensity of laser 2, L2, is controlled to ensure light reaching the photodiodes P1 and P2 are equal.

In other words, if the optical absorbance through path 2 increases, less light impinges on photodetector 2, resulting in higher drive current on laser 2 until photocurrent 2 matches photocurrent 1. Conversely, if the absorbance through path 1 increases, less light impinges on photodetector 1 causing a diminished drive current and intensity on laser 2. Absorbance can then be mathematically inferred from the ratio of light intensities from the respective lasers required to keep photocurrents 1 and 2 equal, and these intensities can be measured directly from the laser modules themselves. Figure 7 is only one portion of the complete circuit used with this device. The anodes of the photodiodes built into the laser modules were multiplexed through an analog switch to the same photoamplifier circuit so that the photocurrents/light intensities of each could independently be measured.

The relationships between media absorbances and measured laser intensities in the setup described above can be derived by first principles. By the definition of light absorbance (Equation 18), the measured absorbances through paths 1 (A_1) and 2 (A_2) can be written respectively as equations 20 and 21.

$$A_1 = \log \frac{I_{O1}}{I_1} \tag{20}$$

$$A_2 = \log \frac{I_{O2}}{I_2} \tag{21}$$

By design the circuit ensures that the light intensities I_1 and I_2 are matched, such that they cancel each other out when taking the difference between A_1 and A_2:

$$A_1 - A_2 = \log \frac{I_{O1}}{I_{O2}} \tag{22}$$

Invoking the Beer-Lambert Law (Equation 19), the difference of absorbances can also be written as

$$A_1 - A_2 = \left(\varepsilon l_y C_{in} + \varepsilon l_x C_{out} + Bf\right) - \left(\varepsilon l_x C_{in} + \varepsilon l_y C_{out} + Bf\right) \tag{23}$$

Simplifying this expression, the biofilm absorbances (Bf) drop out and the absorbance difference between the two light paths is directly proportional to the difference in concentrations C_{in} and C_{out} in the two compartments of the cell:

$$A_1 - A_2 = \varepsilon(l_y - l_x) * (C_{in} - C_{out}) \tag{24}$$

Path lengths l_y and l_x respectively are designed as 1.4 cm and 0.4 cm such that the difference is equivalent to the standard 1 cm path length:

$$A_1 - A_2 = \varepsilon(C_{in} - C_{out}) \tag{25}$$

Relating equations 22 and 25, an expression is found in which the concentration differences in the compartments of the cell is related to the observed laser intensities.

$$A_1 - A_2 = \log\frac{I_{O1}}{I_{O2}} = \varepsilon(C_{in} - C_{out}) \tag{26}$$

Equation 26 illustrates an important relation that demonstrates the functionality of the optical cell and incorporated circuitry. It relates what can be measured, I_{O1} and I_{O2}, to what is desired to be observed: the difference in concentrations of the incoming untreated algae suspension and the treated algae suspension leaving the electrolysis cell.

As seen in equation 23, the device also automatically corrects for biofilm formations as both light paths travel thorough all of the same biofilms. The system can even adapt to various feed concentrations without need of recalibration if a reference optical absorbance cell is attached at the feed of the monitoring optical absorbance cell. The reference cell must have the same orientation as the monitoring cell and have the "treated" chamber filled with algae-free media representing 100% algae removal (Figure 8).

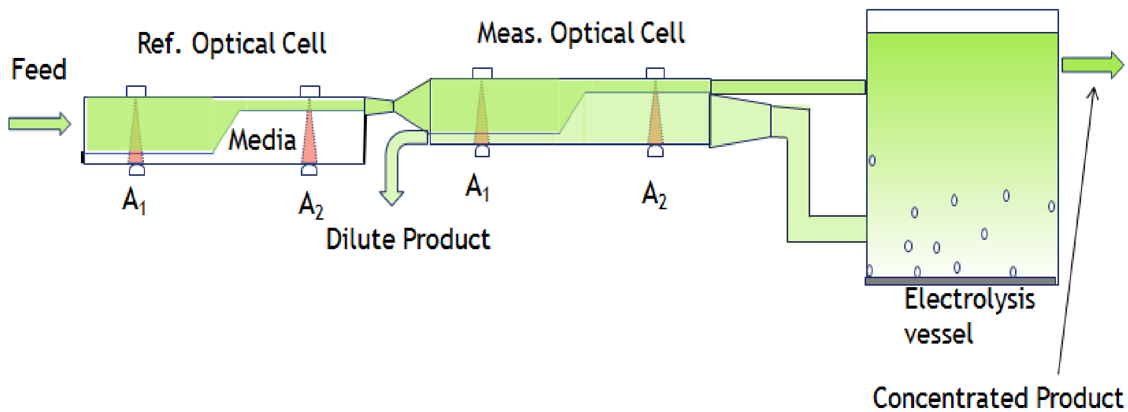

Figure 8. Configuration of Two Optical Cells to Monitor Algae Separation Efficiency in Real-time. Incoming biomass concentration is measured in the reference cell, and biomass removal is measured in the second cell. Note that in practice, the cells were oriented vertically to prevent trapping of bubbles on the cell walls.

By comparing the absorbance differences in the measuring optical cell to the absorbance differences in the reference optical cell, percent removal can be monitored in real-time.

The measured laser intensities were normalized to the values observed when both compartments of the optical cell contained the same reference media to correct for deviations from the designed path lengths, variations in detector sensitivity, and component misalignments. Each optical cell of the custom harvest monitoring device was calibrated with 5 different standards made by diluting stock algae culture in media (100%, 75%, 50%, 25%, and 0% stock culture), using sterile media in the reference chambers. The results from the analysis should give the absorbance of the standard directly corrected for the background absorbance of the media, as the cell was designed to automatically determine the absorbance difference between the fluids in the measured and reference chambers in the cell. For additional validation/evaluation of system performance, the estimated absorbance values of the standards (corrected for background absorbance of the media) were compared to the same measurements made with a commercial spectrophotometer (BioSpec-mini, Shimadzu Scientific Instruments, Kyoto, Japan). Two emission wavelengths were tested with the BioSpec-mini. The first was 650 nm which matched to the lasers in our device. The second was 686 nm which was the peak absorbance wavelength observed for the algae.

5.5. Methods of Bubble Sizing

For acoustic bubble sizing, a 1 MHz transducer with a broad frequency range (IAHG012, NDT Systems, Huntington Beach, CA) was used as a hydrophone to record resonant frequencies of generated bubbles. An impulsive acoustic force was not used to induce bubble oscillations. The method employed was passive and relied solely on oscillation induced from bubble detachment from the electrode surface. A custom amplification circuit was utilized that could amplify the transducer signal by 100x, 1000x, 10000x to make weak signals easier to observe. Signals were analyzed using a Fast Fourier Transform (FFT) function on a digital oscilloscope (Tektronix TDS 2012, Tektronix, Inc., Beaverton, OR). The FFT transforms the signal from a time domain into a frequency domain. By examining the FFT, the predominant bubble size could be determined by comparing the amplitude of the peaks at different frequencies. It was expected that changing the waveform characteristics would shift the predominant bubble size. Below is the acoustic bubble sizing assembly diagram (Figure 9).

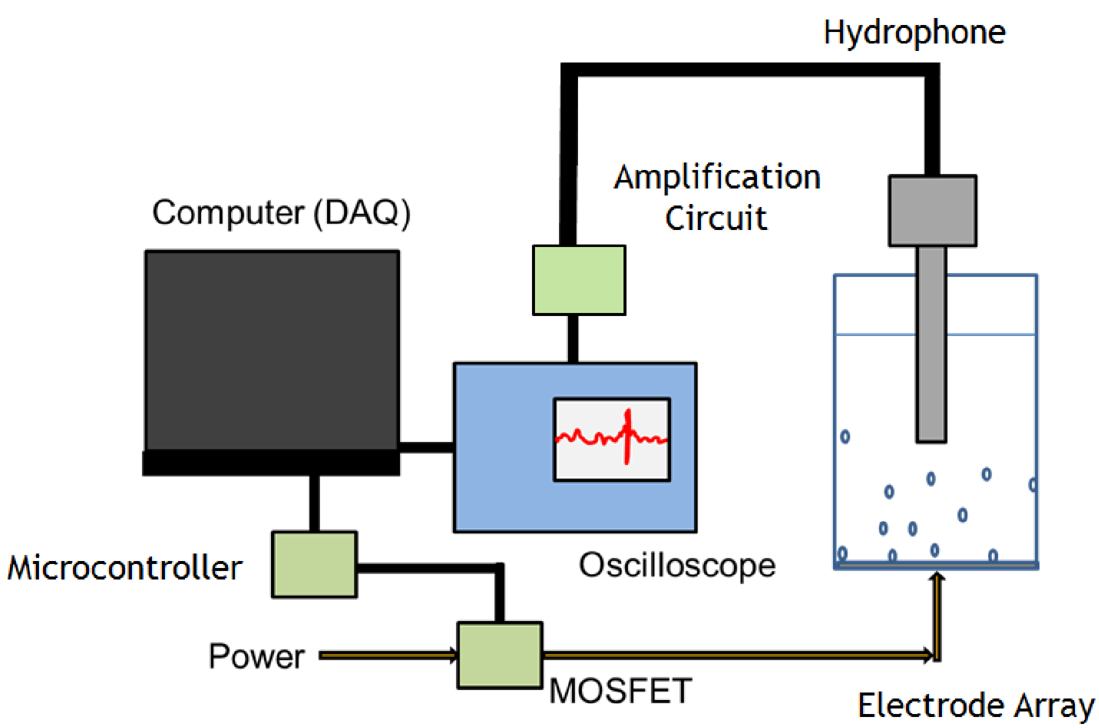

Figure 9. Passive Acoustic Bubble Sizing Assembly Diagram

Some attempts were also made to estimate bubble size distributions through observations of laser diffraction (Spraytec, Malvern Instruments Ltd, Malvern, UK). The system is typically used to measure droplet size in sprays and aerosols but it was thought that it could be used to size bubbles as well. Results from acoustic and light scattering bubble sizing attempts are summarized in section 6.1.

The optical method, although the most time intensive alternative, was the most functional so it was selected. It is discussed in more detail in the following section.

5.6. Bubble Sizing and Gas Generation Efficiency.

Bubble sizing and gas generation efficiency runs were performed in succession (discussed in detail in section 5.6.1). These were separate from the algae separation runs and were conducted using algae-free f/2-Si media (filtered natural seawater collected off shore of the island of Oahu and supplemented with minerals and vitamins as follows: 8.82×10^{-4} M $NaNO_3$, 3.62×10^{-5} M $NaH_2PO_4H_2O$, 1.17×10^{-5} M $FeCl_3$ $6H_2O$, 1.17×10^{-5} M Na_2EDTA $2H_2O$, 3.93×10^{-8} M $CuSO_4$ $5H_2O$, 2.60×10^{-8} M Na_2MoO_4 $2H_2O$, 7.65×10^{-8} M ZnSO4 $7H_2O$, 4.20×10^{-8} M $CoCl_2$ $6H_2O$, 9.10×10^{-7} M $MnCl_2$ $4H_2O$, 2.96×10^{-7} M thiamine HCl (vitamin. B_1), 2.05×10^{-9} M biotin (vitamin. H), 3.69×10^{-10} M cyanocobalamin (vitamin. B_{12})). The seawater was first filtered through a 0.1/0.1 µm pore size filter (AcroPak 1000 Capsule 12999, Pall Corporation, Port Washington, NY). After the media was made, it sat for approximately one week and then was filtered again through a 0.22 µm pore size filter (SCGPU10RE, EMD Millipore, Billerica, MA).This was the same media that the algae were cultured in.

The bubble sizing measurements were made in a continuous flow arrangement. The flow entered the upper port of the electrolysis vessel and exited at the lower port (Figure 10). The fluid level of the vessel was controlled by positioning the outlet flow's tubing at the desired level (Figure 10).

For bubble sizing, high speed video was used. A camera (Rebel T2i, Canon, Inc., Melville, NY) equipped with a microscope adapter (A14CN305, Cyber Scientific Inc., Kitchener, Ontario) was connected to a microscope (Sixty Spencer, American Optical Company, Buffalo, NY). The magnification was approximately 130x. The objective was 10x but the adapter was rated as 12x-15x depending on the camera CMOS sensor. This was the magnification description of the adapter provided by the manufacture. The objective lens of the microscope was centered 5.2 cm above the electrode array.

To estimate energy required for electrolysis, electrical voltage and current were measured during the electrolysis runs. The amount of current supplied to the electrolysis cell was communicated serially from the programmable power supply to a PC. All the current supplied to the electrode array was sourced from the power supply. The Arduino controller was powered by its own supply, using a common ground to enable switching of the MOSFET.

Gas generation was monitored by fitting the electrolysis cell with a sealing lid and adding an additional volume displacement vessel (modified 50 mL centrifuge tube) (Figure 10). The gas generated during electrolysis would collect in the confined space at the top of the displacement vessel and displace water from it. The water displaced from the vessel was directed through another tube into a receptacle on a scale (Adventurer

ARA520, Ohaus, Pine Brook, NJ), and data from the scale was communicated serially to the PC. The weight of water displaced was used to estimate the amount of gas generated and later converted to a molar basis from the ideal gas law and assuming 1 atm ambient pressure. Both the electrical current and gas displacement (scale measurements) were recorded every second using a custom “virtual instrument.” configured with commercial software (LabVIEW 8.5, National Instruments, Austin, TX).

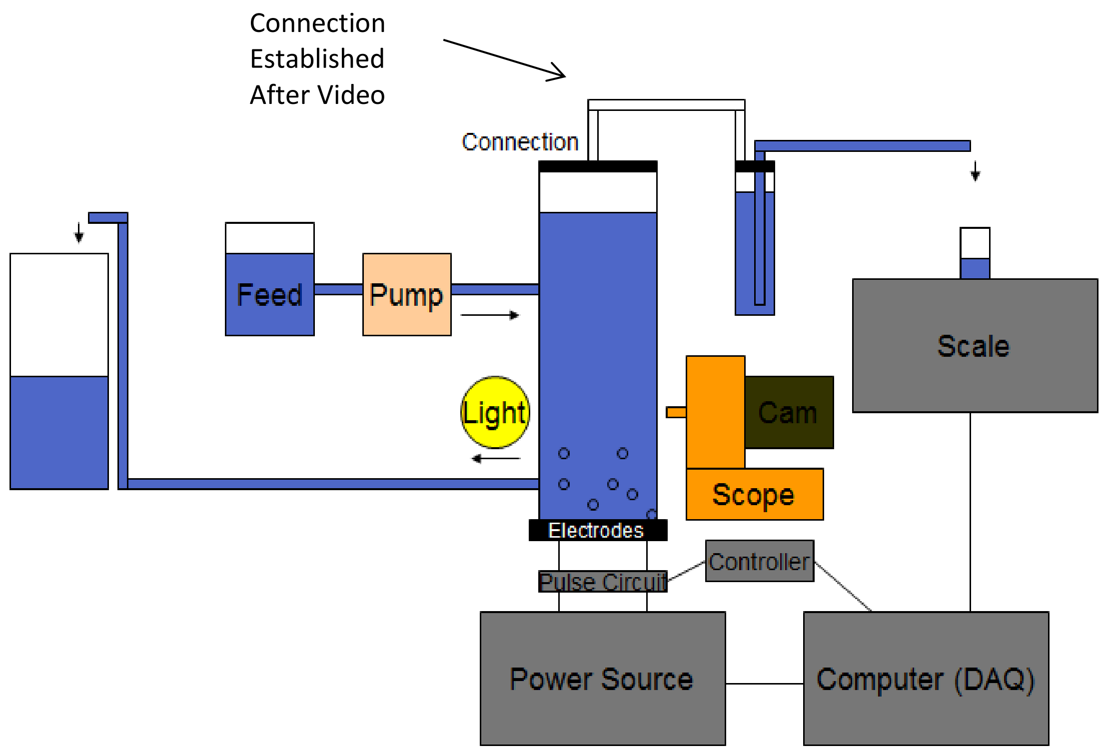

Figure 10. Bubble Sizing and Gas Generation Monitoring Assembly Diagram

The outlet height coming off the displacement vessel was slightly elevated (approximately 7.6 cm) in relation to the surface liquid level of the displacement vessel.

This resulted in a small amount of head pressure over ambient to be overcome for displacement of water. Also, the air space above the liquid in the displacement cell was not held at a fixed level. Inconsistent air spaces combined with the small amount of head pressure may have added to the variability in the measured gas generation rate. This was not expected to have a significant impact on results. Atmospheric pressure was not recorded on testing days and this may have contributed to variability in gas generation rates estimated on a molar basis from the ideal gas law.

5.6.1. Bubble Sizing and Gas Generation Efficiency Test Procedure

The bubble sizing and gas generation test began with setting the voltage on the power supply and uploading the desired waveform parameters to the microcontroller. The electrolysis cell was filled with 220±5 mL f/2-Si media and the pump started (23 mL min.$^{-1}$ corresponding to a residence time of 9.6 minutes). The electrical connection between the electrolysis cell and the pulse current circuit was established and a warm up to steady state period, minimum of 30 seconds not exceeding 3 minutes, was allowed to proceed. High speed video was recorded after the warm up phase and recording continued until a minimum of 100 unique bubbles in focus were visually observed. Directly after recording video, the pump was stopped, the outlet flow was plugged, and the top gas outlet of the electrolysis cell was connected to the displacement cell (if video was less than 1 minute, waiting until 1 minute had passed was performed before this step). Recording current and scale measurements (once every second) was then started. After the first drop from the displacement vessel landed in the beaker on the scale, current recording and scale measurements were continued for 1 minute.

5.6.2. Bubble Sizing and Gas Generation Efficiency Analysis Procedure

Recorded video from each run was reviewed frame by frame until 100 bubbles in focus were found. Those images were imported into an image analysis software (ToupView, AmScope, Irvine, CA) to size the bubbles. ToupView counts pixels to size objects given a reference object of known dimensions. For reference, a microscope slide with 100 µm gradations was used to establish the scale. Diameters of spherical bubbles and the smallest center dimension across on oval bubbles were recorded (Figure 11).

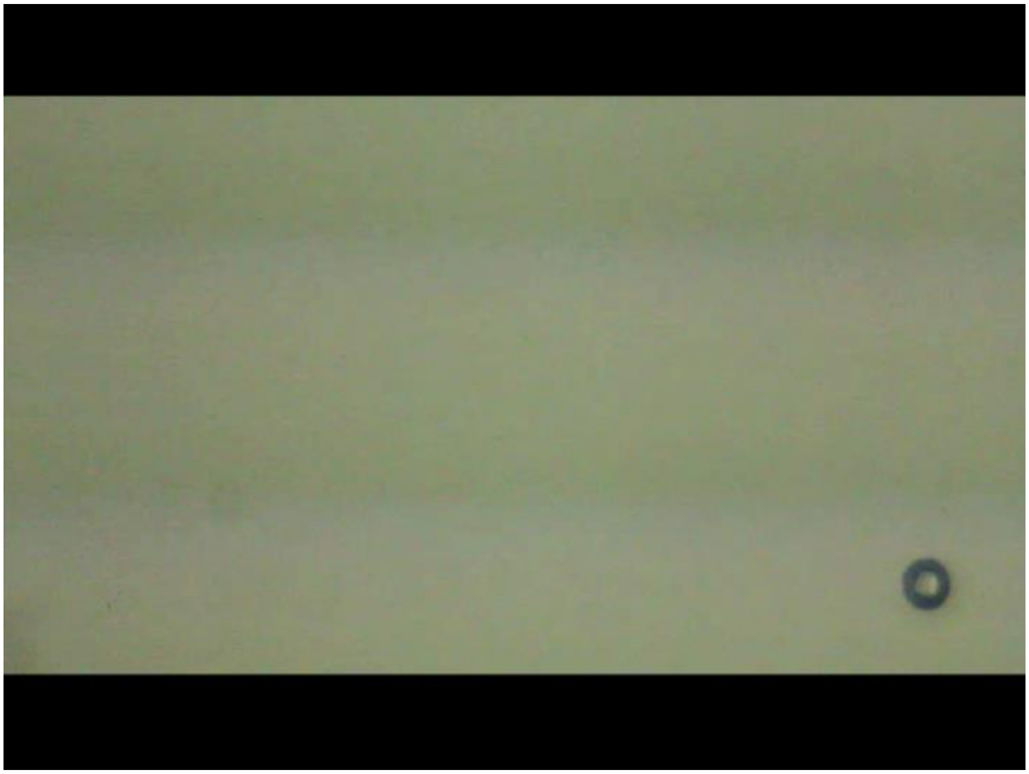

Figure 11. Example Image from High Speed Video Showing an Electrolysis Generated Bubble in Focus. Image was recorded during a run at 3 V, 10%, 25 Hz, and observed bubble size was estimated to be 43.6 μm

For some bubble sizing runs, particularly runs with vigorous electrolysis, images were dark and grainy due to the high shutter speed required to take 30 frames per second, and dispersion/occlusion of light through the thick clouds of bubbles. In these cases, finding 100 unique bubbles in sharp focus in the recorded footage was not possible. Below, Figure 12, is an example image of what was considered the threshold of a bubble in acceptable “focus”.

Figure 12. Bubble Focus Threshold Example. Image demonstrates the limit on what was accepted as “in focus.” (picture taken from a 6V,20%, 100Hz run)

This subjective visual standard was applied to all runs so that 100 unique bubbles could be sized. Grainy bubbles were sized by selecting the darkest observable edges of the bubble. This may overestimate bubble size and bias data from treatments where more dark and grainy images were present (e.g. 6V DC and 6V, 20% duty cycle treatments).

Gas generation efficiency was estimated by processing the data collected during the final minute of the gas generation runs. Electrical power (Watts) delivered to the electrolysis cell was estimated as the product of the average current and the applied potential.

The volumetric rate of gas generation was determined in excel by least squared error linear regression of the weight measured by the scale vs. time. Assuming the density of water to be 1 g cm^{-3}, converting the volumetric displacement to molar generation rate of gas was achieved based on the ideal gas law assuming standard temperature (298 K) and ambient pressure (101.325 kPa). By dividing the molar gas generation rate by power, molar gas generation efficiency (mol J^{-1}) was estimated.

5.7. Algae Separation

In this section, the algae culture characteristics, culturing methods, algae separation test procedure, and total biomass separation analysis are described.

5.7.1. Algae Culture

Marine *Chlorella* sp. were selected as the model microalgae for electroflotation runs. *Chlorella* spp. are green, unicellular microalgae (Bishop and Zubeck, 2012) and generally range in size from 2-15 µm (Sanyano et al., 2013). The specific microalgae used in our investigation were readily available from the collection of a collaborator at UH, and could be rapidly cultivated for us, but has not yet been fully characterized and the exact species is unknown. *Chlorella* spp. are often used for nutraceuticals (Bishop and Zubeck, 2012) and biodiesel production (Chisti, 2007) making them worth investigating as model organisms.

A marine species of microalgae was selected because electroflotation of a marine strain of microalgae hasn't been investigated before. Marine media has a potential advantage in that it would have a higher electrical conductivity than fresh water media. Higher electrical conductivity results in less resistance within the electrolysis cell and consequently gas generation occurs at a lower energy cost. There is the potential drawback however of oxidative damage to the algae cells from the generated chlorine gas reacting with water to form hypochlorite (a strong oxidizer). We hypothesized that electroflotation rates would be efficient enough that oxidative damage would be mitigated.

Algae were cultured in 1 L batches in f/2-Si media in a Percival E-22L incubator (Percival Scientific, Perry, IA), on a cyclic 12:12 lighting schedule (lights (Hygrade F17T8/741/ENV Hg, SATCO, Brentwood, NY) turn on at 6 a.m., gradually increase intensity till noon, ramp back down to dark at 6 p.m.). Maximum light intensity was 85-100 umol (m^{-2} s^{-1}). The algae were used approximately one and a half weeks after inoculation which was when the algae were assumed to have reached their plateau concentration. Approaching testing days, batches were transferred to a 20 W fluorescent light grow station (continuous light) (Grower's Supply Co., Dexter, MI). The algae were then used in runs approximately 24 hours later.

5.7.2. Algae Culture Total Suspended Biomass Test Procedure

To further understand the properties of the algae suspension, a representative culture was analyzed for total suspended solids (TSS). The TSS content was assumed to be entirely composed of biomass. The background corrected optical density of this reference culture was used to estimate the TSS of other cultures analyzed throughout the runs based on their measured optical densities by single point calibration, and it was assumed that the entire TSS fraction was composed of algal biomass. From this information, energy input per dry material or lipids recovered could be estimated.

TSS contents of the reference culture was estimated on the basis of mass captured on tared 1 µm pore size filters (1821-090, Whatman, Pittsburgh, PA). 200 mL of culture were sucked through the filters mounted in a Buchner funnel using a laboratory vacuum source. To wash off residual salts and minerals from the marine media, 200 mL of deionized distilled water was also sucked through the treated filters. After washing the filters, they were dried for 1 hour in a furnace (47900, Barnstead and Thermolyne , Dubuque, IA) set at 105° C, then allowed to cool in a glass desiccator for 30 minutes prior to recording the final weights (Adventurer AR2140, Ohaus, Pine Brook NJ). The difference between the final and initial weights of the filters divided by the 200 mL culture volume provided the concentration in grams of dry biomass per milliliter.

5.7.3. Algae Separation Test Procedure

Due to the occurrence of algae bleaching during electrolysis which resulted in large biases in optical measurements used to estimate algae concentrations, it was not possible to get reliable measurements of harvest efficiency using our custom optical instrument (more algae bleaching details are provided in section 6.4.3). As an alternative, algae separation runs were conducted in 5 minute 220 ± 5 mL batch runs, and flotation efficiency was estimated based on off-line optical density measurements of different fractions collected manually from the flotation cell. One fraction collected was the foam/top fraction and the other was the bulk fraction. By comparing the different fractions' optical measurements at the end of the run, the optical measurement bias due to algae bleaching was avoided. This is because the bleaching is assumed to affect the top and bulk fractions equally. Current was also monitored during these runs in the same manner as during the gas generation efficiency portion of the bubble sizing and gas generation efficiency runs.

The algae separation runs began with setting the voltage on the power supply and uploading the desired waveform parameters to the microcontroller. The electrolysis cell was filled with 220±5 mL of algae culture. The cell was then connected to the pulsed current circuit and current measurements were recorded every second during the entire run. At 5 minutes, the electrolysis cell was disconnected from the pulse current circuit. Any generated foam was immediately collected with a spoon and transfer into a 15 mL centrifuge tube. 8 mL from the surface was removed using a pipette and transferred in to the same tube. 8 mL of bulk sample was also collected through the lower flow port. This fraction was stored in a seperate 15 mL centrifuge tube.

5.7.4. Biomass Separation Analysis

For treated cultures, optical density was used as a proxy for the relative biomass content of different fractions. Two replicate readings were made of each sample at 686 nm, using sterile media as the reference. Each replicate was prepared by transferring 2 ml of sample from the centrifuge tubes to a clean cuvette following 5 seconds of vortexing.

A simple material balance was performed to calculate the percent recovery of algae from suspension (Equation 27). A_t and A_b are the measured absorbances of the top and bulk fractions.

$$\% \text{ biomass recovery} = \left(\frac{\mathrm{A_t}*(8\text{ mL})-A_b*(8\text{ ml})}{\mathrm{A_t}*(8\text{ mL})+\mathrm{A_b}*(212\text{ mL})}\right)*100 \qquad (27)$$

The numerator in equation 27 represents the total biomass recovered in the foam and the denominator represents the total biomass in the entire cell. The right hand term in the numerator is to account and correct for the biomass present in the top 8 mL of treated culture used to resuspend the foam fraction.

Equation 27 is an approximation of the actual percent recovery. The equation assumes that the bulk fraction is a homogeneous suspension but in reality a concentration gradient forms (higher concentrations in upper sections) inside the column during flotation. The potential bias of not fully considering the concentration gradient on the calculated biomass recovery overestimates biomass recovery. Determining the gradient was not experimentally simple or feasible.

5.7.5. Seawater Electrolysis and Algae Bleaching Analysis Procedure

In our experiments, we observed cellular bleaching and destruction. To examine this effect in greater detail, an experiment was designed to measure changes in visible/optical properties of bulk cultures exposed to a batch electroflotation process. For this experiment, the procedure outlined in the Algae Separation Test Procedure section of this report (5.7.3) was followed up to step 5, using a 3 V DC treatment. After step 5, the foam was not collected off the top surface of the electrolysis vessel. Instead the entire contents, foam and bulk, were remixed back together, and the absorbance compared to that of the original culture, scanning wavelengths from 400 to 900 nm (scans were corrected for the background absorbance of sterile media). These spectra were recorded to help determine if damage was occurring to chlorophyll and other pigments, and/or if there was an overall drop in turbidity resulting from the electroflotation process.

Further review of cell degradation due to algae bleaching was also performed by optical observations. The treated and untreated algae cultures were centrifuged (Centrifuge 5415 D, Eppendorf, Hamburg, Germany) at 1500 x g to concentrate the algae cells. Nearly all supernatant was removed by pouring. The concentrated samples were observed through a microscope (Labomed Lx400, Labomed Inc., Los Angeles, CA) and photographed (Figure 29).

The same experimental procedure followed to evaluate the bleaching and cell disruption of 3 V DC electrolysis was also conducted at 6 V, 20%, 100 Hz with the exception that only optical observations were made for this additional set of conditions.

5.8. Lipid Separation Analysis Procedure

The remaining volume in each 15 mL centrifuge tube after the biomass separation analysis was 4 mL. These 4mL sample volumes were refrigerated overnight before performing the lipid separation analysis. To start the analysis, the remaining volume left in a 15 ml centrifuge tube was sonicated (Microson Ultrasonic Cell Disrupter, Misonix, Farmingdale, NY) for 1 minute in an ice bath at a power level of 11 W. This was to lyse the algae cells and disperse lipids throughout the media. 1 mL aliquots of sample were immediately transferred with a micropipette into three 3 mL centrifuge tubes. One tube was used as a background and the other two were analyzed for lipid content with the lipid stain Nile red. 2 µL of 1 mM Nile red in DMSO were added to one of the 1 mL aliquots. To mix the sample with the Nile red solution and to emulsify the lipids with the aqueous phase, the aliquot was immediately sonicated for approximately 5 seconds at the same intensity used to lyse the algae cells. 200 µL were immediately transferred with a micropipette into a cuvette and put in the fluorometer (F-2500, Hitachi, Tokyo, Japan). At an excitation wavelength of 530 nm, an emission scan from 560 nm to 800 nm was performed. Fluorescence values and wavelengths of the peak emissions were recorded for each scan. The analysis process for each experimental treatment sample was performed in replicate. The background tube followed the same process with the exception that it was not stained with Nile red. See Figure 13 for a visual representation of this procedure.

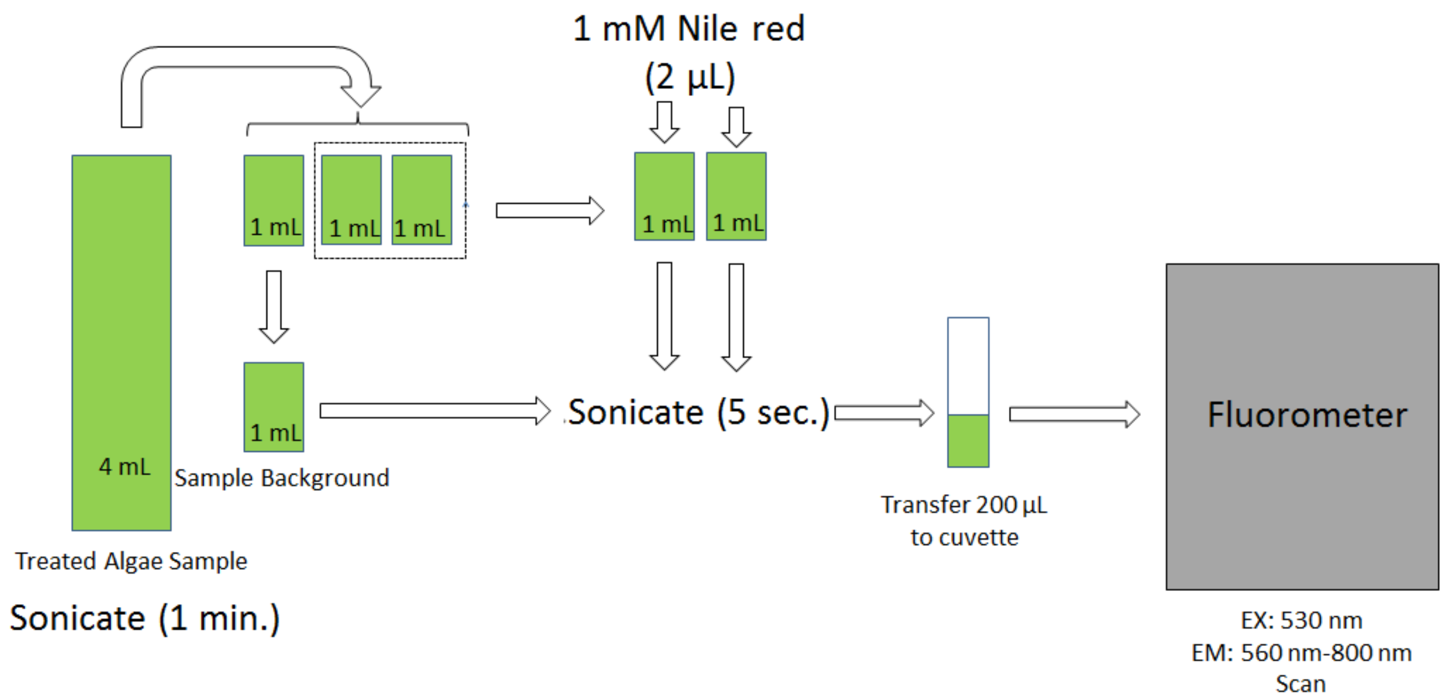

Figure 13. Process for Analyzing Lipid Content of Samples. Only one 1 ml aliquot is processed at a time.

Fluorescence emission scans of each sample without Nile red stain were recorded to correct for any intrinsic fluorescence in the samples. Scans were also recorded of the sterile media stained with Nile red to correct for media-stain interactions in the absence of lipids. Three replicates of the stained sterile media were analyzed and fluorescence values averaged to use for correction of all samples.

Percent recovery of lipids was analyzed in the following manner. Fluorescence values and wavelengths at peak emissions of replicate aliquots within the same treatment sample were averaged together. Corrections were determined from fluorescence values of the backgrounds (aliquot not stained with Nile red, and media stained with Nile red) taken at the average wavelength where the peak fluorescences in the stained duplicate aliquots were located. The fluorescence values on both backgrounds were subtracted from the averaged sample peak fluorescence to get the final corrected fluorescence. Lipid contents in samples were assumed to be directly proportional to the corrected fluorescence values.

A simple material balance was performed to calculate the percent recovery of lipids from suspension. An equation analogous to Equation 27, substituting corrected fluorescence values in the top and bottom fractions for the corresponding absorbance values in those fractions, was used to estimate the percent lipid recovery.

5.9. Experimental Design

A 2^3 factorial arrangement was used to evaluate the effects of 3 factors, applied potential (V), duty cycle (%), and frequency (Hz), with a minimal number of experiments

(Table 1). Factorial arrangements are useful in reducing the number of runs required to understand the effects of the factors studied (Box et al., 2005). To identify factors and interactions with statistically significant effects, data were analyzed using custom excel worksheets to perform an Analysis of Variance (ANOVA), requiring replication of every treatment to estimate overall experimental error. As a baseline comparison for each applied potential level, electroflotation experiments were also performed using DC current at those potentials.

Table 1. 2^3 Experimental Design. Orders in this table were used for the bubble sizing and gas generation efficiency runs. New randomized orders were created for the biomass and lipid separation runs.

				First Order		Results		
	Order		Frequ.	Duty Cycle	Voltage			
Run	Rep. 1	Rep. 2	A	B	C		Rep. 1	Rep. 2
1	7	10	-1	-1	-1	**3V, 10%, 25Hz**		
2	4	1	1	-1	-1	**3V, 10%, 100Hz**		
3	6	5	-1	1	-1	**3V, 20%, 25Hz**		
4	2	3	1	1	-1	**3V, 20%, 100Hz**		
5	10	7	-1	-1	1	**6V, 10%, 25Hz**		
6	1	9	1	-1	1	**6V, 10%, 100Hz**		
7	3	2	-1	1	1	**6V, 20%, 25Hz**		
8	8	8	1	1	1	**6V,20%, 100Hz**		
3V DC	5	6				**3V DC**		
6V DC	9	4				**6V DC**		

Coded Variables	-1	1
Frequency: A	25 Hz	100Hz
Duty Cycle: B	10%	20%
Applied Potential: C	3V	6V

For initial selection of experimental levels, the only factor reviewed by preliminary parametric tests was applied potential to find the minimum voltage required to generate directly observable bubbles. Finding the minimum voltage required to generate bubbles was necessary because it was desired to set the low applied potential treatments near this value. Approximately 2.0 V was found to be the level at which bubbles could first be observed in the f/2-Si media. Therefore the low applied potential level was set to 3 V and the high applied potential was set to 2x this value (6 V). As previously mentioned in section 4.4.2, experimental levels for frequency and duty cycle were selected in relation to published values in the literature resulting in a reducing effect on bubble sizes.

6. Results and Discussion

The following section discusses the bubble sizing, gas generation efficiency, biomass separation, and lipid separation results and observations. Also, calibration of the real-time microalgae harvest efficiency monitoring device is reviewed.

6.1. Bubble Sizing Methods Results

Syringe tests in the absence of electrolysis with various gauge needles were used to generate bubbles for preliminary evaluation of passive acoustic bubble sizing. Syringe test results were promising with smaller bubbles producing signals with shifts into higher resonance frequencies as expected (Figure 14).

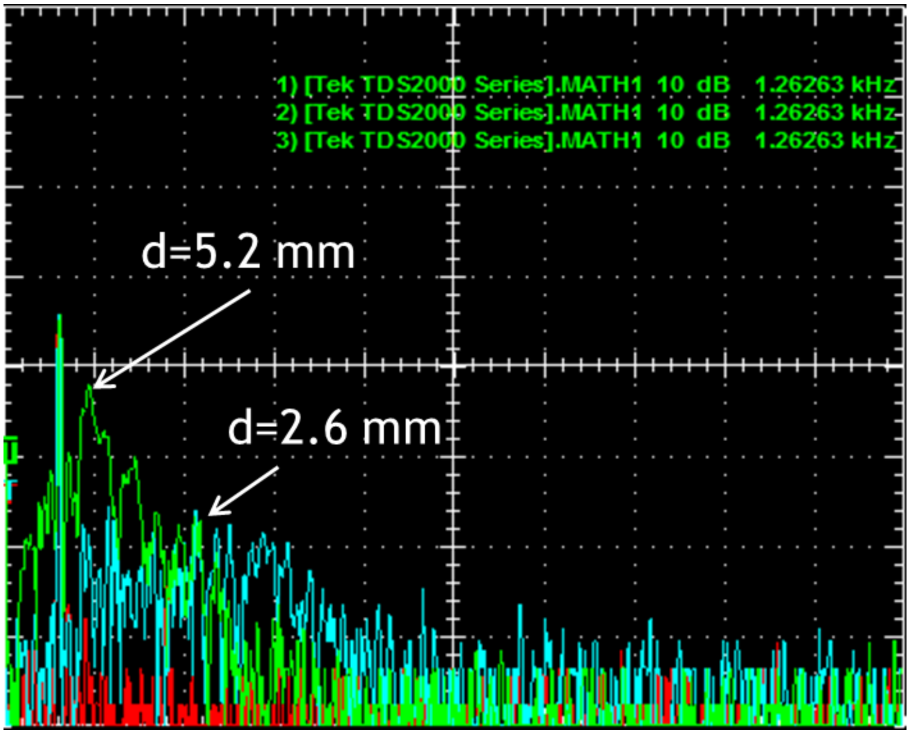

Figure 14. FFT of Syringe Tests. 1000x signal amplification. 1.26263 kHz per major horizontal division, 10 dB per major vertical division (0 dB = 1 V_{RMS})

In Figure 14, the red signal is the background, the green signal corresponds to the bubbles produced by the thick gauge needle, and the blue signal corresponds to the bubbles produced by the thin gauge needle. The bubble diameters corresponding to the labeled peaks in Figure 14 were estimated from the Minnaert Equation (17). Optical verification (EX-F1, Casio, Tokyo, Japan) was used to confirm that acoustic estimated bubble diameters were reasonable.

Unfortunately the hydrophone and circuit amplification was not sensitive enough to detect small bubbles especially at small volumetric generation rates. Electrolysis runs at higher potentials (4.5-6 V) and constant DC produced vigorous electrolysis. Vigorous electrolysis under these conditions produced distinguishable signals from the background, but electrolysis at low (3 V) applied potentials with pulsed current conditions did not produce distinguishable signals from the background. Furthermore, acoustic energy is biased towards larger bubbles so that detailed quantitation of bubble size distributions could not be directly determined from the FFT spectra.

The Spraytec runs were unsuccessful in bubble sizing runs. The bubble plume was simply too dense for the instrument to execute measurements.

Because video analysis was the only bubble sizing approach that resulted in reliable data for all experimental conditions, it was used for bubble sizing in all of the factorial experiments for this investigation.

6.2. Bubble Sizing Results

The experimental conditions resulting in the smallest observed mean bubble diameter were 3 V, 20%, 25 Hz with a diameter of 30.1 µm (Figure 15).

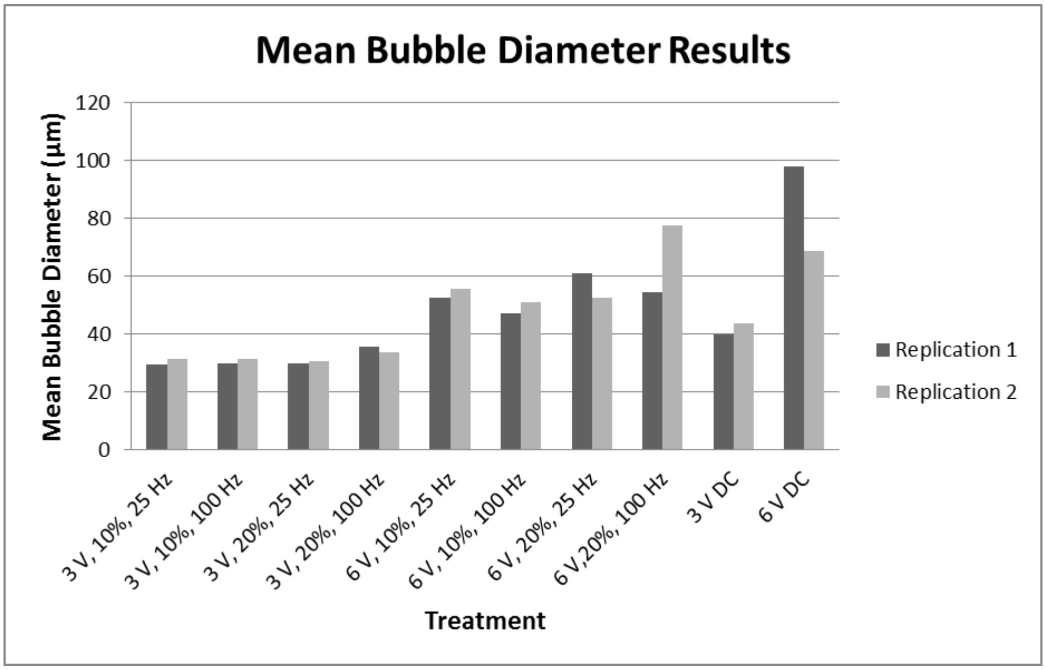

Figure 15. Mean Bubble Diameter Results

Pulsed current conditions typically resulted in smaller mean bubble sizes when compared to bubbles generated from the corresponding DC applied potential (e.g. 3 V pulsed vs 3 V DC and 6 V pulsed vs 6 V DC). Changing the applied potential had a significant effect on bubble size. Increasing the applied potential increased the mean bubble diameter (Figure 15).

The ANOVA indicates that applied potential is the only significant factor affecting mean bubble size at the 0.05 significance level (Table 2).

Table 2. Mean Bubble Diameter ANOVA. Green highlights the significant factor.

Source	df	SS	MS	F	F (0.05)
Total	15	3159.60			
Treatment	(7)				
A (Frequency)	1	20.29	20.29	0.51	5.32
B (Duty Cycle)	1	138.62	138.62	3.46	5.32
C (Applied Potential)	1	2503.76	2503.76	62.49	5.32
AxB	1	88.35	88.35	2.20	5.32
AxC	1	0.23	0.23	0.01	5.32
BxC	1	62.44	62.44	1.56	5.32
AxBxC	1	25.38	25.38	0.63	5.32
Error	8	320.53	40.07		

This is peculiar because changing duty cycle and frequency both lead to differing "off" times to provide opportunity for bubble detachment which was expected to affect the bubble sizes.

Median bubble diameters from different experimental treatments were also compared (Figure 16).

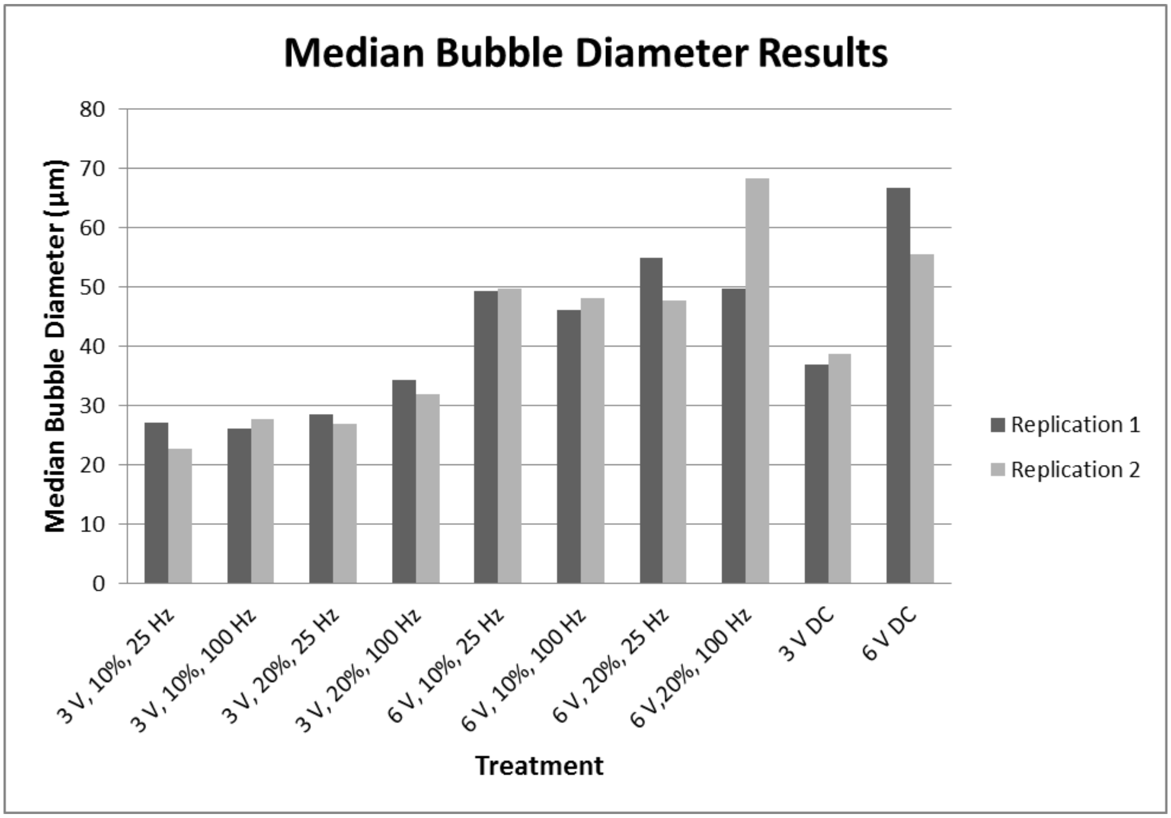

Figure 16. Median Bubble Diameter Results

The experimental conditions resulting in the smallest median bubble diameter were 3 V, 10%, 25 Hz at 25.0 µm.

Once again, only applied potential was found to be significant in the ANOVA (Table 3).

Table 3. Median Bubble Diameter ANOVA. Green highlights the significant factor.

Source	df	SS	MS	F	F (0.05)
Total	15	2667.73			
Treatment	(7)				
A (Frequency)	1	39.93	39.93	1.46	5.32
B (Duty Cycle)	1	127.84	127.84	4.66	5.32
C (Applied Potential)	1	2217.76	2217.76	80.92	5.32
AxB	1	44.39	44.39	1.62	5.32
AxC	1	0.96	0.96	0.04	5.32
BxC	1	5.72	5.72	0.21	5.32
AxBxC	1	11.85	11.85	0.43	5.32
Error	8	219.27	27.41		

In reviewing the shape of the bubble size distributions (Figures 17 and 18), one will see a different trend in the effects of current pulsing in the 3 V runs and 6 V runs.

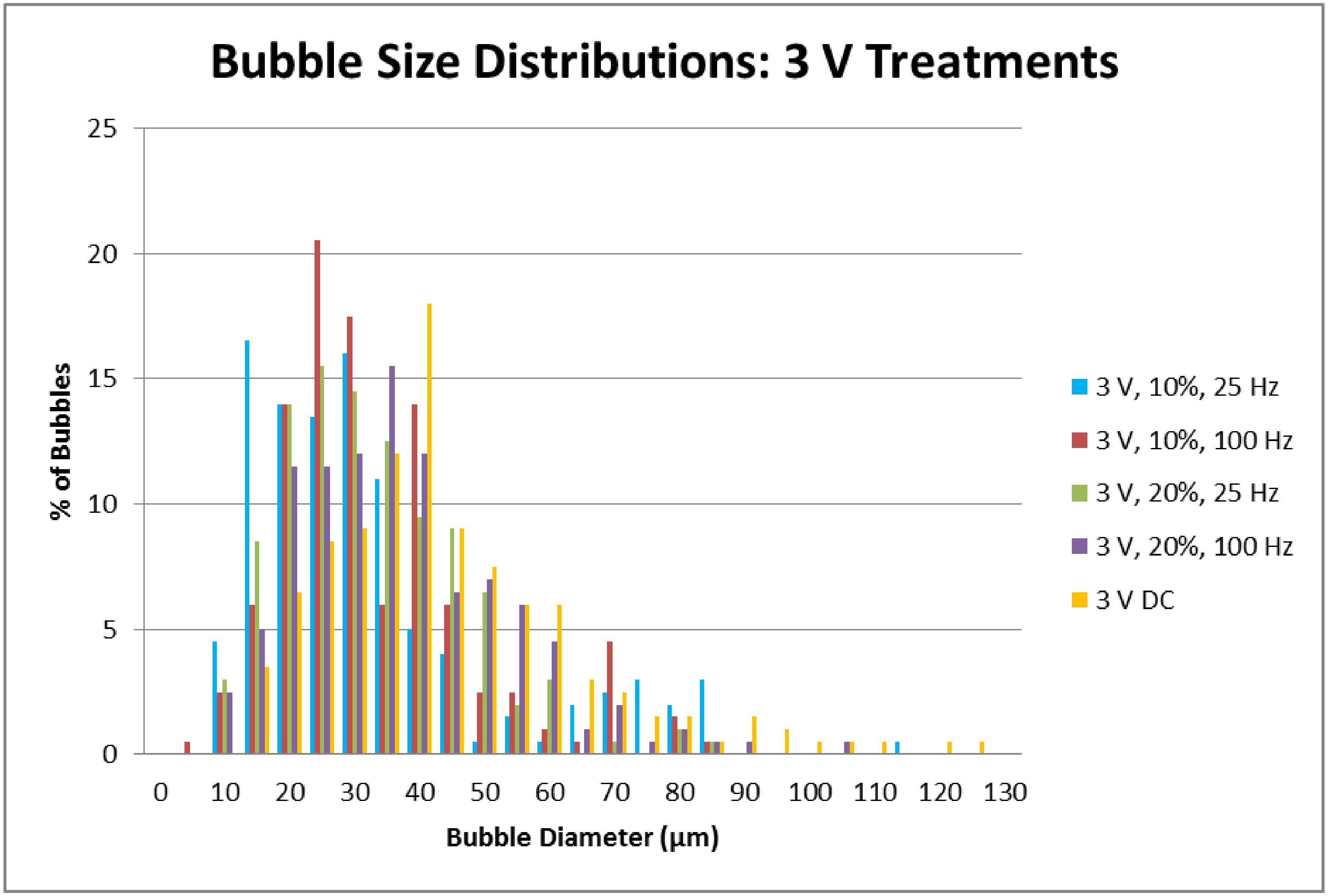

Figure 17. Distribution of Pooled 3 V Treatments

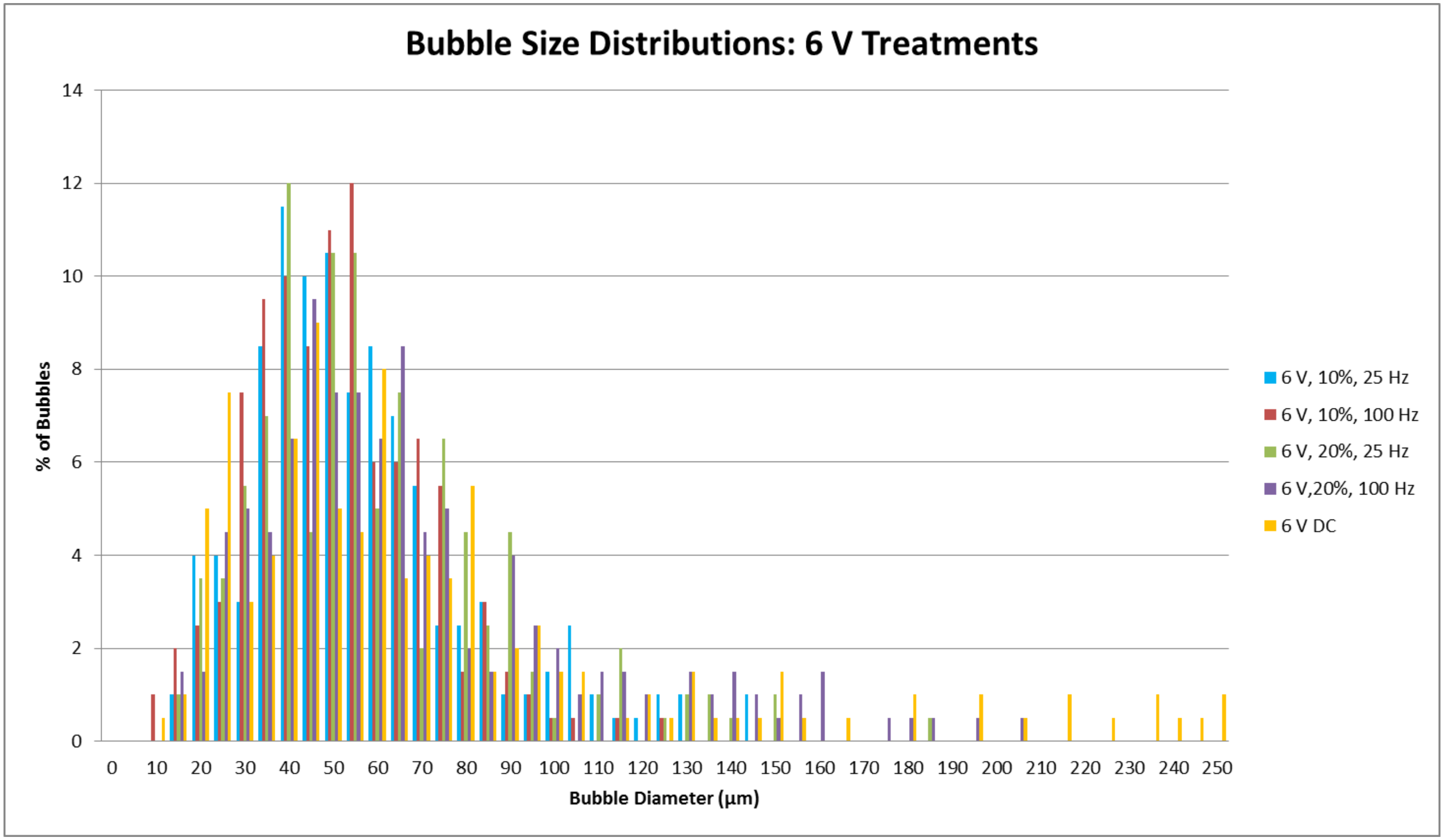

Figure 18. Distribution of Pooled 6 V Treatments. 94% of the 6 V DC bubbles were less than or equal to 250 µm with the largest observed bubble being 359.4 µm. All other runs have bubble sizes that fall within the range of the graph. The range from 0-250 µm was selected to best graphically display all the run results.

In the 3 V runs, the distributions shift towards smaller bubble diameters resulting in an increase in the number of smaller bubbles being generated during pulsed runs. This trend was similar to what was observed in a study by Khosla et al. (1991). For 6 V runs, this trend was not observed however. Instead what was most noticeable for the 6 V runs was the increased uniformity of bubble size using pulsed electrolysis. The distributions of the 6 V pulsed runs were much narrower with fewer large outlier bubbles than the distribution of the 6 V DC runs (Figure 18). To further illustrate these differences, standard deviations of the distributions were calculated from the 100 bubble measurements for each run and then averaged across the two replicates (Table 4).

Table 4. Average Standard Deviations for Treatment Bubble Size Distributions

	Mean (µm)	Median (µm)	Average Distribution Standard Deviation (µm)
3 V, 10%, 25 Hz	30.33	24.96	19.66
3 V, 10%, 100 Hz	30.64	27.00	15.13
3 V, 20%, 25 Hz	30.08	27.81	13.46
3 V, 20%, 100 Hz	34.75	33.07	16.16
3 V DC	41.75	37.79	19.89
6 V, 10%, 25 Hz	54.15	49.52	25.01
6 V, 10%, 100 Hz	48.95	47.14	19.83
6 V, 20%, 25 Hz	56.77	51.32	28.23
6 V,20%, 100 Hz	66.01	59.04	35.40
6 V DC	83.38	61.13	71.93

The standard deviations of bubble diameters for the 6 V pulsed runs were all at least two times smaller than the standard deviation of the 6 V DC run.

When increasing the applied potential from 3 V to 6 V, the current increased as well (Table 5).

Table 5. Average currents recorded during electrolysis conducted under different experimental conditions.

	Average Current (A)
3 V, 10%, 25 Hz	0.025
3 V, 10%, 100 Hz	0.023
3 V, 20%, 25 Hz	0.043
3 V, 20%, 100 Hz	0.031
3 V DC	0.069
6 V, 10%, 25 Hz	0.129
6 V, 10%, 100 Hz	0.151
6 V, 20%, 25 Hz	0.273
6 V,20%, 100 Hz	0.302
6 V DC	1.494

Higher currents (directly related to higher current densities) were correlated with larger bubble sizes (Figure 19).

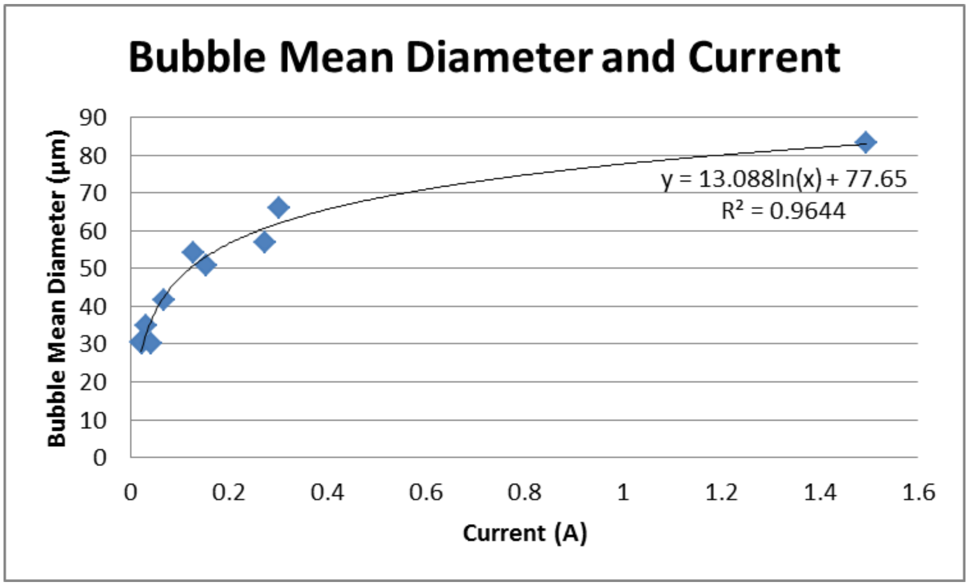

Figure 19. Correlation Between Bubble Mean Diameter and Current

The observed trend of higher currents producing larger bubbles is not consistent with other data reported in the literature. For example, Sarkar et al. (2010; 2011) demonstrated that current density had no influence on hydrogen bubble sizes produced. Khosla et al. (1991), reported that bubble size actually decreased with higher current densities.

Our investigation differs in a number of ways from the investigations mentioned above. First, they were only examining hydrogen bubbles generated from a platinum cathode. I was simultaneously recording bubbles generated from both cathodic and the anodic currents on DSA electrodes. Secondly, they were not operating in a marine environment. The marine environment could contribute to a further degree of supersaturation because it has a higher ion concentration meaning more energy is available for electrochemical conversion and not wasted on conductive losses in the media. Also, our electrolysis cell's tight electrode spacing may have resulted in a further degree of supersaturation than what others' cells did.

6.2.1. Seawater Electrolysis and Cathodic Mineral Scaling

Electrolysis in a marine environment will produce mineral scale deposition at the cathode (Belmont et al., 1998). This scale is composed of hydroxides, $Mg(OH)_2$ and $Ca(OH)_2$, and can passivate the surface of the electrode (Belmont et al., 1998). Scaling occurred in our electrolysis runs as well (Figure 20).

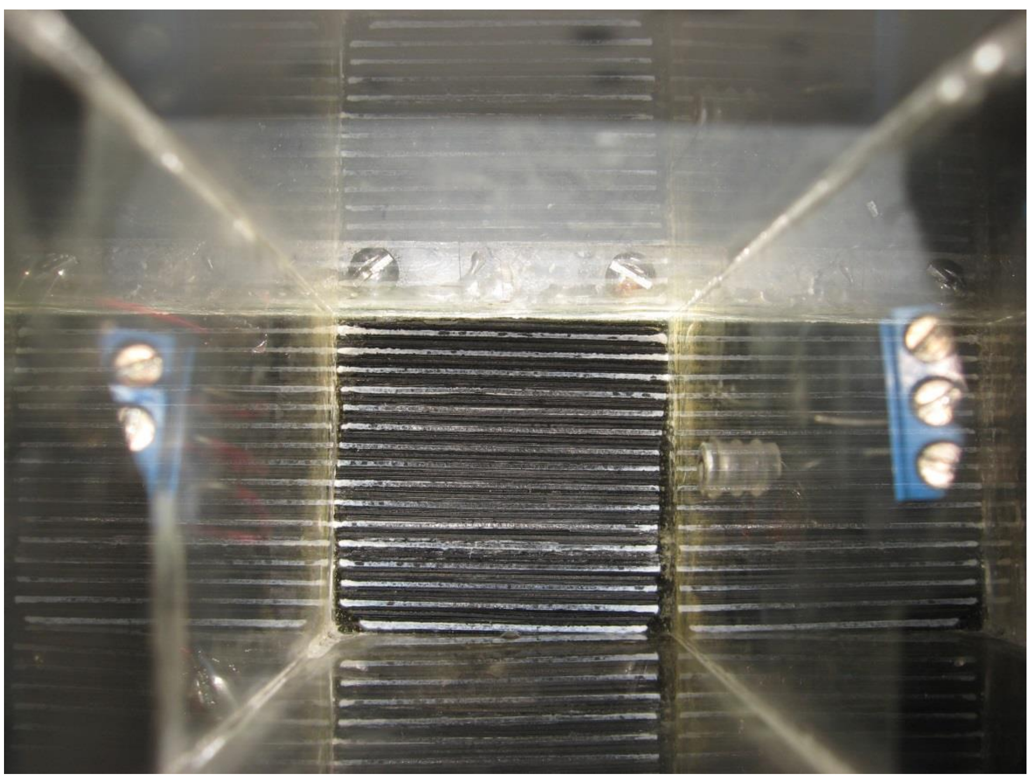

Figure 20. Scaling on Cathodes After Marine Electrolysis. The white deposits are the scales.

This scaling effect may have contributed to variability in all experiments. This is especially true for bubble sizing runs as the electrode surface morphology is a critical factor. If scale detached from the electrode, it could also affect absorbance measurements. Brushing and scrubbing with sponges was attempted to reduce scale formation. More consistent and effective cleaning of electrodes is recommended for future testing.

6.3. Gas Generation Efficiency Results

In reviewing Figure 21, the current is noisy and peak amplitudes are not consistent.

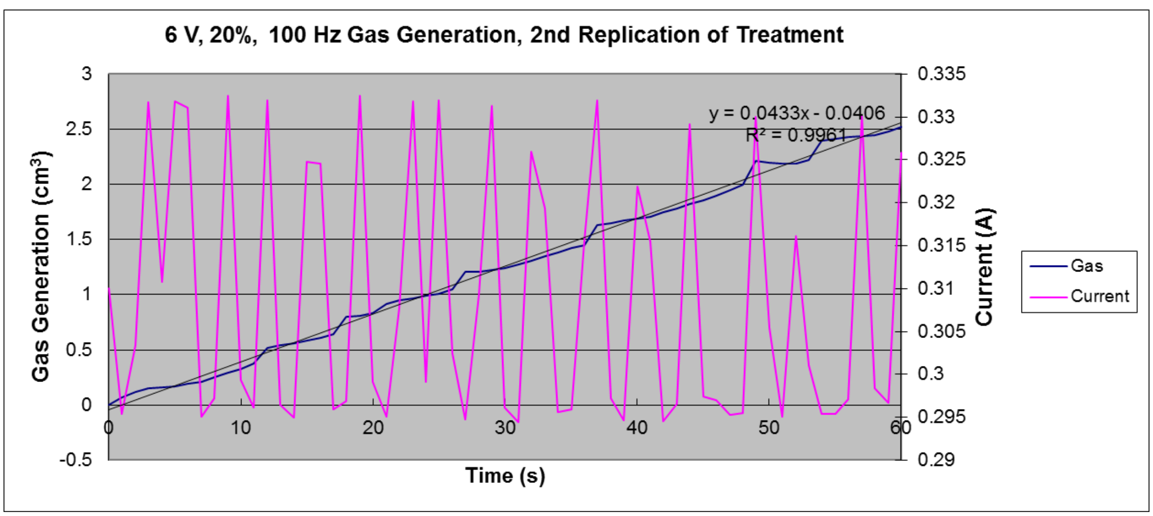

Figure 21. Example of Gas Generation Efficiency Data

These observations suggest that the sampling rate and dynamic response of the current meter (including analog to digital conversion) were not well suited for reliable estimation of the average currents under the pulsing conditions of these experiments. On one hand, the dynamic response of the current measurement appears to be too slow to accurately measure the rapidly pulsing current as many of the instantaneous current measurements have transitional values between zero and the peak observed value. On the other hand, the dynamic response is fast enough that individual measurements do not accurately reflect average currents such as might be the case with integrating type analog to digital converters with integration periods covering multiple pulse periods. These limitations may have resulted in the measured current deviating from the true mean current as the instantaneous current readings from the meter lagged behind the true values of the rapidly changing current (case d., Figure 22), and samples were recorded infrequently when compared with the periods at which current is pulsed. Our measurement methods are represented by the grey dot (case e., Figure 22). With the medium fast analog to digital conversion and extremely low sampling rate of 1 Hz, the measured data point could be anywhere along the red dotted line (case d., Figure 22).

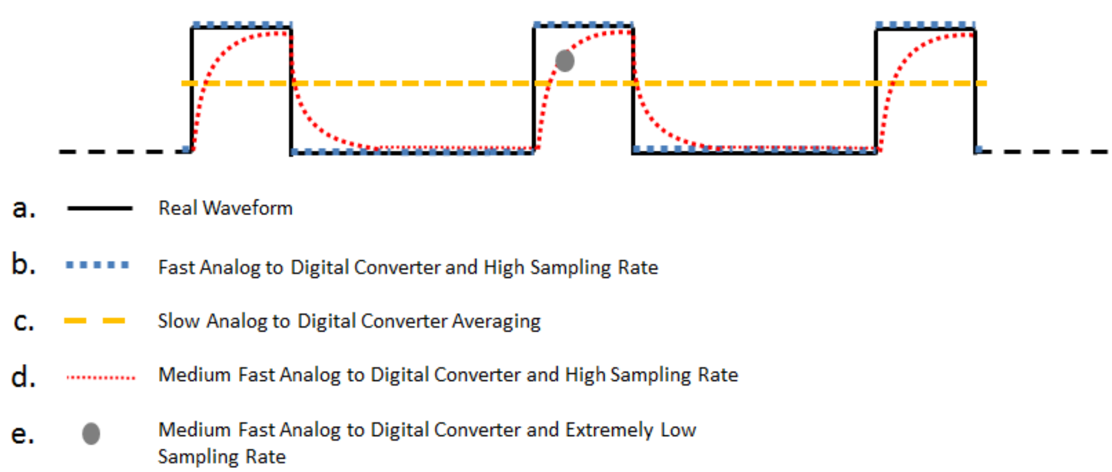

Figure 22. Effects of Analog to Digital Conversion Speed and Sample Rate on Measured Data

Another issue discovered with relying on the power supply for measuring current was that occasionally small offset currents were indicated when the supply was not connected to any load. This current bias was sometimes relatively significant, up to 23% of the average current, for 3 V runs. Correction for this bias was not possible because it was transient and decreased variably with time. The gas generation efficiency could be underestimated especially for 3 V conditions with small amounts of gas generation.

The gas generation efficiency for 3 V DC and 6 V DC were 1.69×10^{-6} mol J^{-1} (average of two runs) and 1.07×10^{-6} mol J^{-1} (average of two runs). For DC electrolysis, lower applied potential is clearly the most thermodynamically efficient method for gas generation. 3 V DC was even found to be the most efficient treatment for generating gas (1.69×10^{-6} mol J^{-1}) (Figure 23).

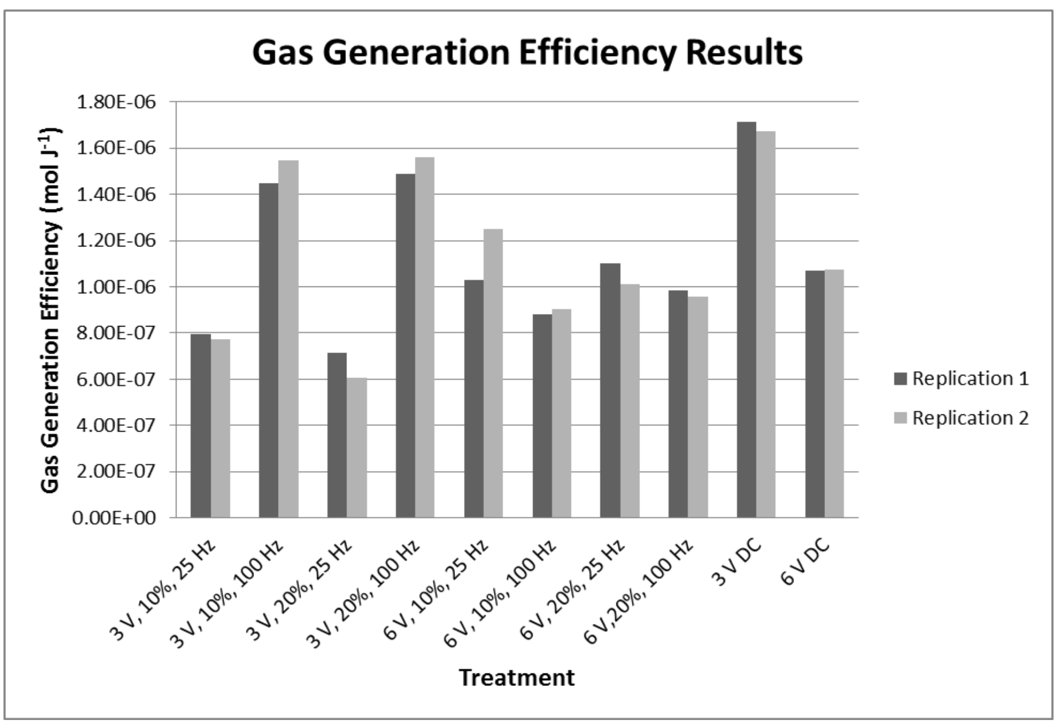

Figure 23. Gas Generation Efficiency Results

Since electrolysis is slower at the smaller potential, the pulsed runs at 3 V result in even less gas saturation and bubble nucleation, and greater amounts of gas diffusion away from the electrode surface.

Considering only the gas generation efficiencies, electrolysis would be conducted at low applied potentials as near as possible the relative redox potentials of the half reactions at the respective electrodes. However, considering that the gas generation rates approach zero at this limit, thermodynamic efficiency of gas generation needs to be balanced against the need for rapid biomass recovery in a practical sized electrolysis cell.

The ANOVA for gas generation efficiency indicated that applied potential was a significant factor at the 0.05 significance level, frequency was a significant factor at the 0.05 significance level, and the applied potential-frequency interaction was significant at the 0.05 significance level. Duty cycle was not found to be significant (Table 6).

Table 6. Gas Generation Efficiency ANOVA. Green highlights significant factors and interactions

Source	df	SS	MS	F	F (0.05)
Total	15	1.41E-12			
Treatment	(7)				
A (Frequency)	1	3.85E-13	3.85E-13	71.91	5.32
B (Duty Cycle)	1	2.73E-15	2.73E-15	0.51	5.32
C (Applied Potential)	1	4.09E-14	4.09E-14	7.64	5.32
AxB	1	2.35E-14	2.35E-14	4.39	5.32
AxC	1	9.11E-13	9.11E-13	170.23	5.32
BxC	1	2.20E-15	2.20E-15	0.41	5.32
AxBxC	1	1.40E-17	1.40E-17	0.00	5.32
Error	8	4.28E-14	5.35E-15		

Frequency was the most significant factor for gas generation efficiency (Table 6) but responses differed between 3 V and 6 V applied potentials. In 3 V runs, increasing the frequency from 25 Hz to 100 Hz had a positive effect on increasing gas generation efficiency. In 6 V runs the inverse was true (Figure 23).

This may be because at 3 V applied potential, 25Hz does not provide as high a degree of saturation as the 100 Hz runs. In this case, more gas diffuses into the bulk and does not contribute to bubble formation and growth. For the higher applied potential, 6 V, reactants are depleted more rapidly and gas saturation occurs to a higher degree. Higher applied potentials combined with higher frequencies may not allow for reactant replenishment within the depleted region near the electrode-electrolyte interface. The increased thickness of the depleted region may lead to more gas being dissolved in the bulk.

6.4. Algae Separation Discussion

In this section, the algae culture total suspended biomass results, the real -time microalgae harvest efficiency monitoring device calibration results, algae bleaching, and biomass separation results are reviewed.

6.4.1. Algae Culture Total Suspended Biomass Results

The batch of algae used in the TSS analysis had an average absorbance of 0.42 (typical algae culture absorbances used in runs were approximately 0.26). The algae suspension was analyzed in triplicate and one sterile media volume was analyzed to account for non-algal suspended solids. The average algae concentration for the tested batch was 0.0001 g ml^{-1}.

6.4.2. Real-time Microalgae Harvest Efficiency Monitoring Device Calibration

Although the response of the custom spectrophotometer was linear with algae concentration (Figure 24), the magnitudes of the measured absorbance values were about 5x lower than reported by the commercial spectrophotometer(Figures 24 and 25).

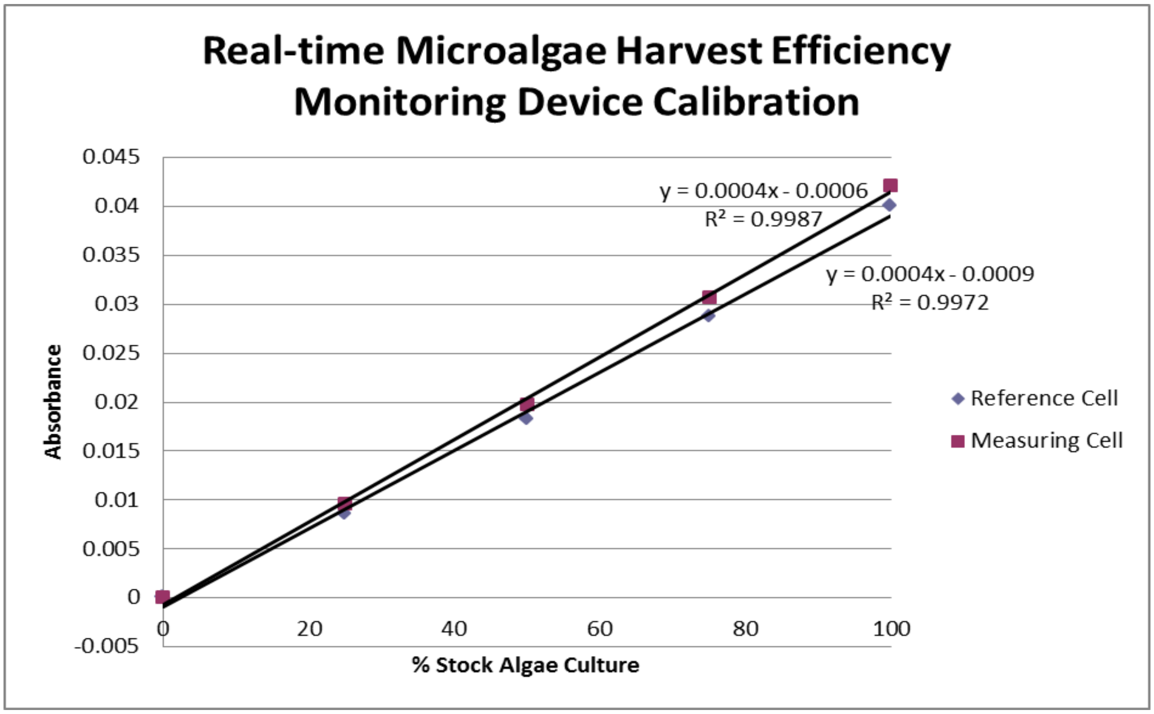

Figure 24. Custom Real-time Harvest Monitoring Device Calibration

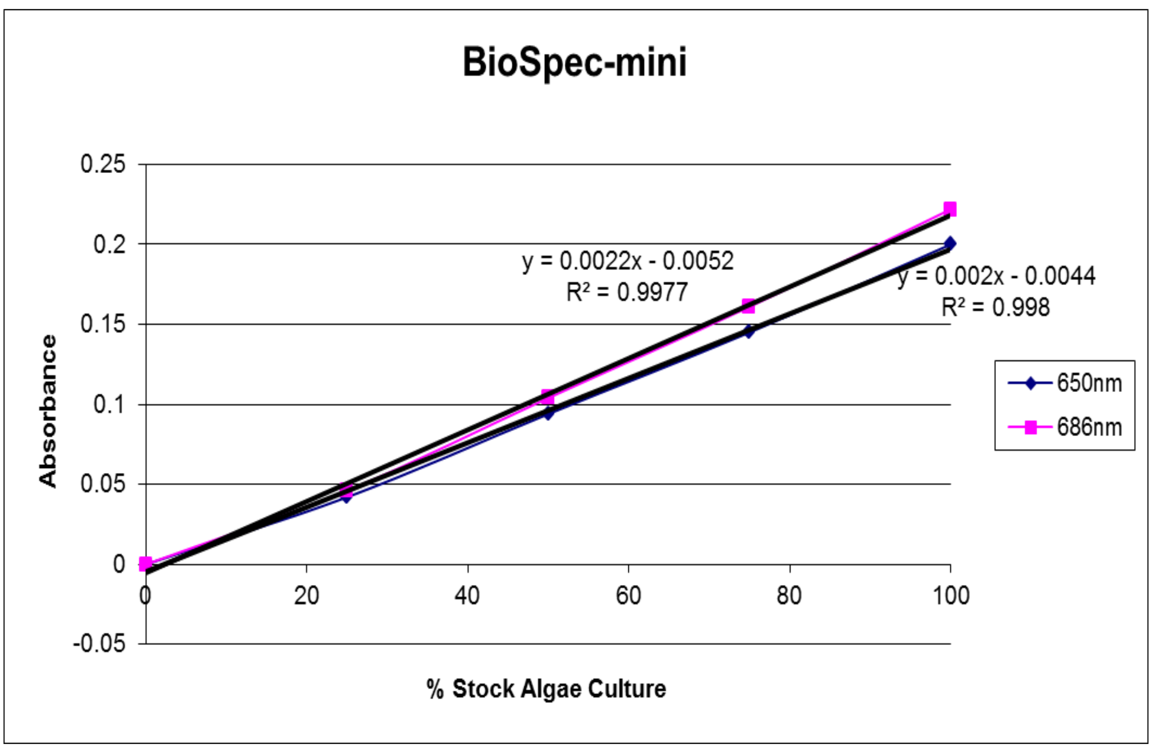

Figure 25. BioSpec-mini Comparison Results

It is currently hypothesized that leakage currents from one photodiode to the other may have occurred in the back-to-back configuration (Figure 7) used for these experiments limiting the sensitivity of our device. To correct this problem other members of the lab are currently evaluating an alternative configuration using the same basic approach but in which the photodiodes drive individual photoamplifiers, with the signals compared in a subsequent summing junction. However, the use of this system for this particular research project was not pursued because the electrolysis conditions in the marine media generated significant quantities of reactive chlorine species which rapidly bleached out the pigments in the algae and appeared to disrupt algae cells, resulting in significant biases in real time measurements (i.e., the treated culture was significantly less optically absorbent than the untreated culture, but these measurements did not reflect the actual biomass content in the treated culture) . As a result, the measurements of biomass separation relied on off-line measurements after batch processing. These results are summarized in section 6.4.4.

6.4.3. Seawater Electrolysis and Algae Bleaching

During preliminary algae separation runs with the custom real-time harvest efficiency monitoring device, it was observed that algae bleaching was occurring. For the runs that produced foam, there was little to no observable green color to the foam (Figure 26 and 27). The green color was also noticeably diminished in the bulk suspension (Figure 26).

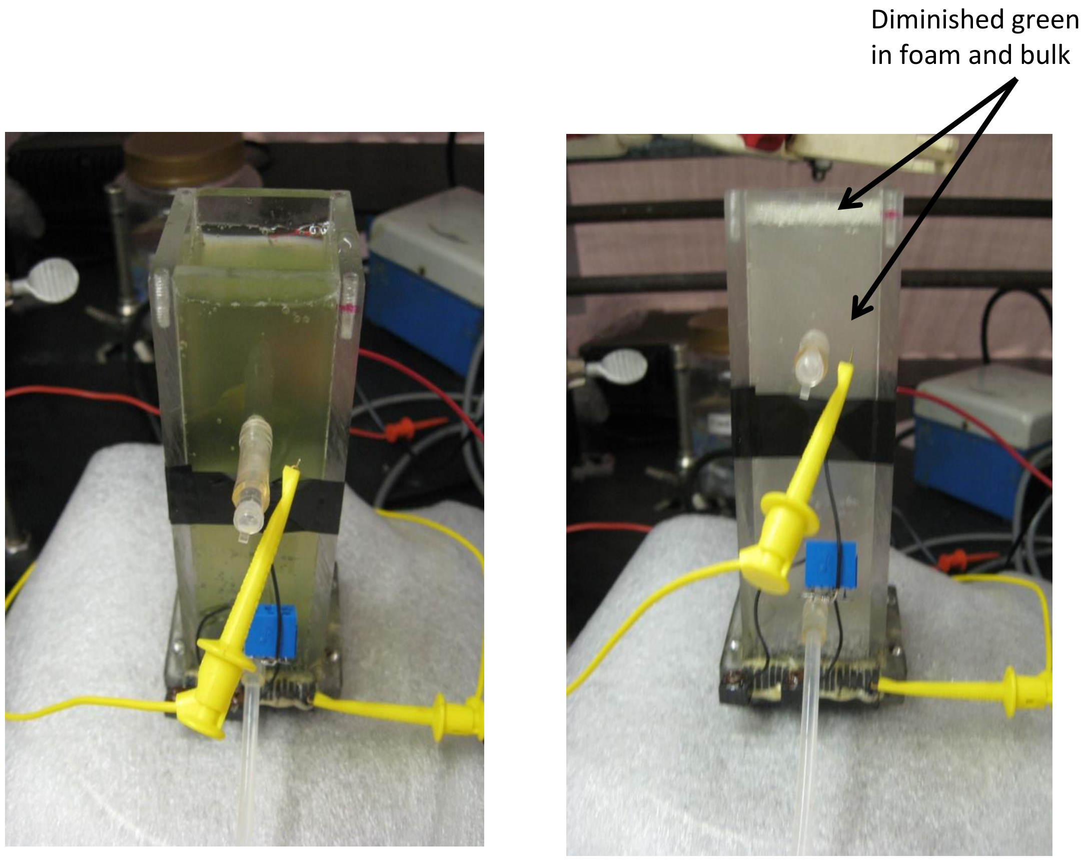

Before

After

Figure 26. Example of Algae Bleaching from 1st Algae Separation Replication: 6 V, 20%, 25 Hz. 5 minute batch run.

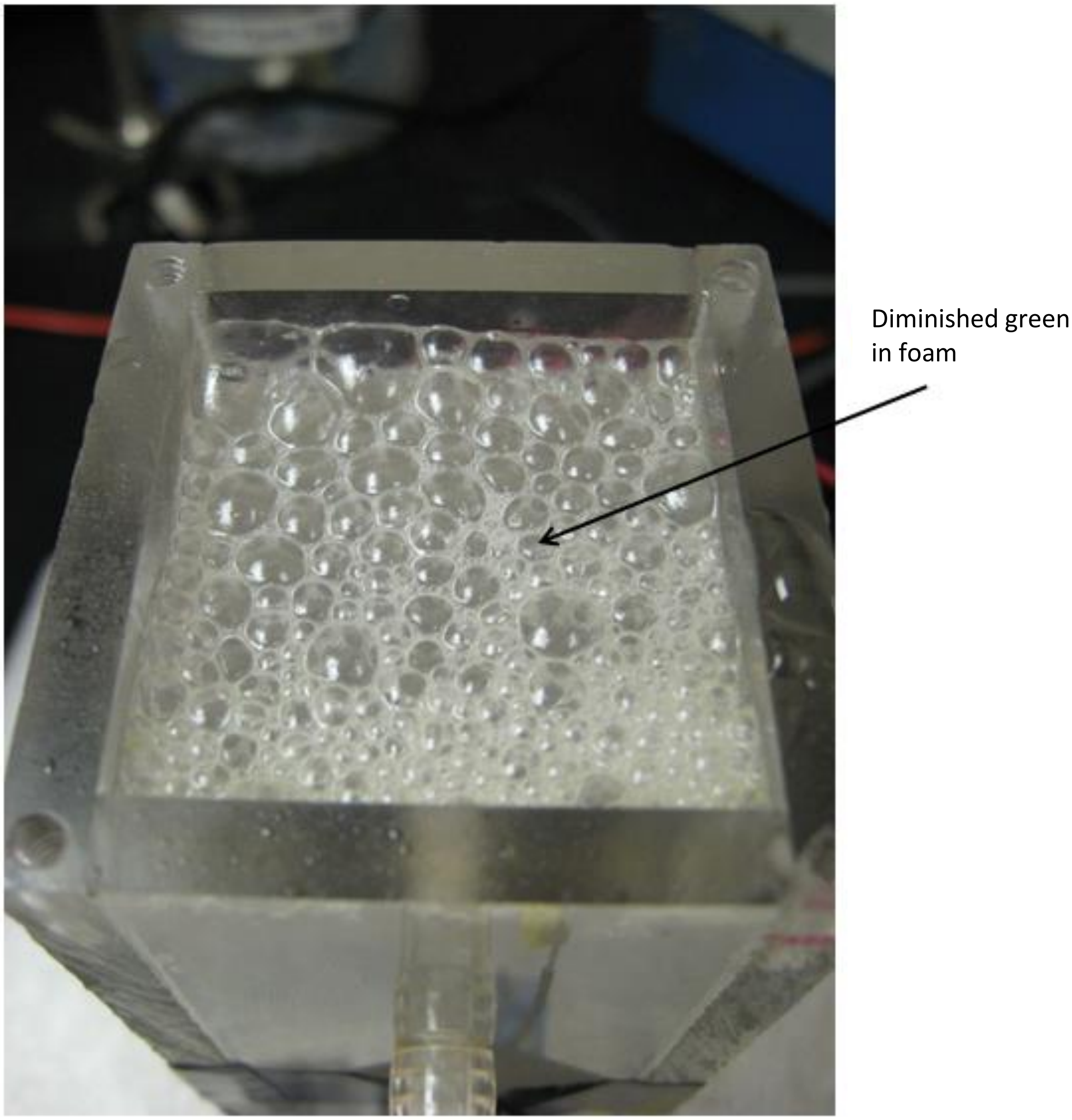

Figure 27. Example of Algae Foam Bleaching from 1st Algae Separation Replication: 6V, 20%, 25Hz. 5 minute batch run.

As previously mentioned, electroflotation of a marine strain of microalgae hasn't been reviewed before and it was assumed that algae recovery might be possible with relatively small amounts of gas generation and relatively little active chlorine degradation effects on the algae. A chlorine smell was observed during runs however and our system and test conditions likely generated substantial quantities of chlorine gas for recovery of suspended algae. A portion of chlorine gas may have reacted in the media to produce hypochlorite (ClO^-) and other reactive chlorine species and potentially oxidized algae cells. The procedure for investigating algae bleaching (Section 5.7.5) was performed after it became evident that algae bleaching and cell disruption were likely occurring. From the absorbance scan for the 3 V DC run, there was a drop in absorbance across the entire wavelength range for the treated algae (Figure 28).

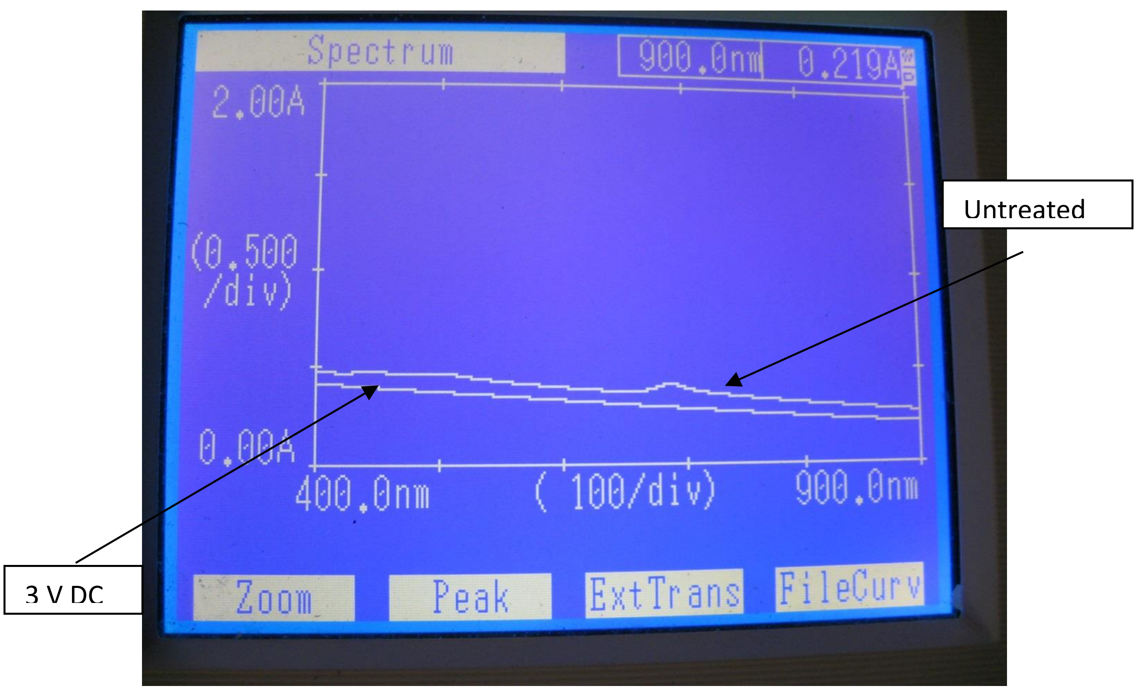

Figure 28. Absorbance Spectra of 5 Minute 3 V DC Electrolysis Run Sample. Contents remixed after run

The reduced overall turbidity could be an indicator that cell lysis is occurring. The local peak at 686 nm putatively corresponding to chlorophyll was not present in the treated culture suggesting that chlorophyll was oxidized. For the hypochlorite to oxidize the chlorophyll, the cells must have undergone a certain degree of lysis or at a minimum the cell wall had to be compromised to allow penetration of hypochlorite.

The microscope images provide the most compelling evidence that cellular damage and lysis result from the electroflotation process in a marine media (Figures 29 and 30).

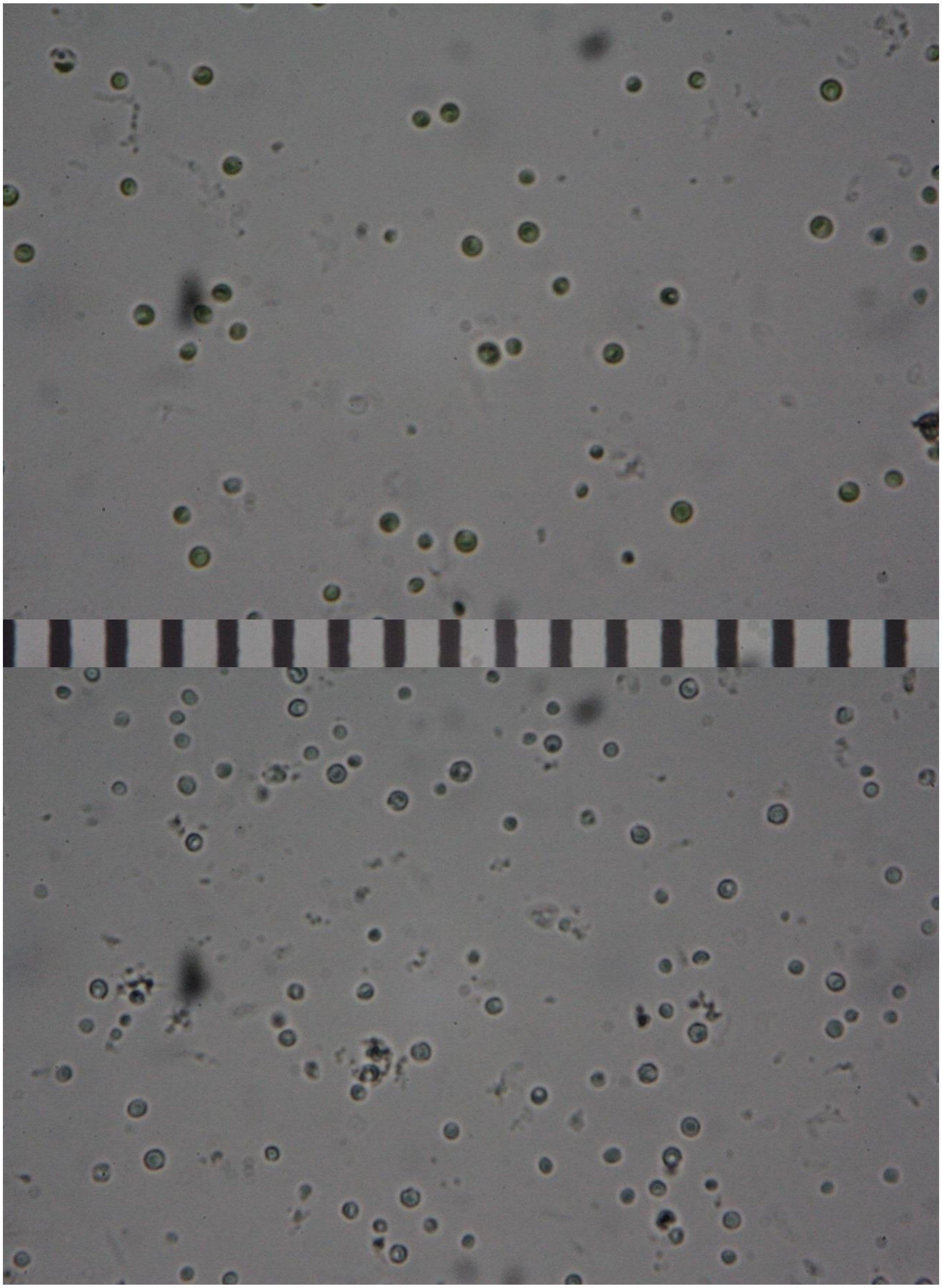

Figure 29. Microscope Images of Untreated Algae and 3 V DC Treated Algae. Top picture is untreated algae, bottom picture is a 5 minute batch run: 3 V DC remixed.
1 division on scale is 10 µm

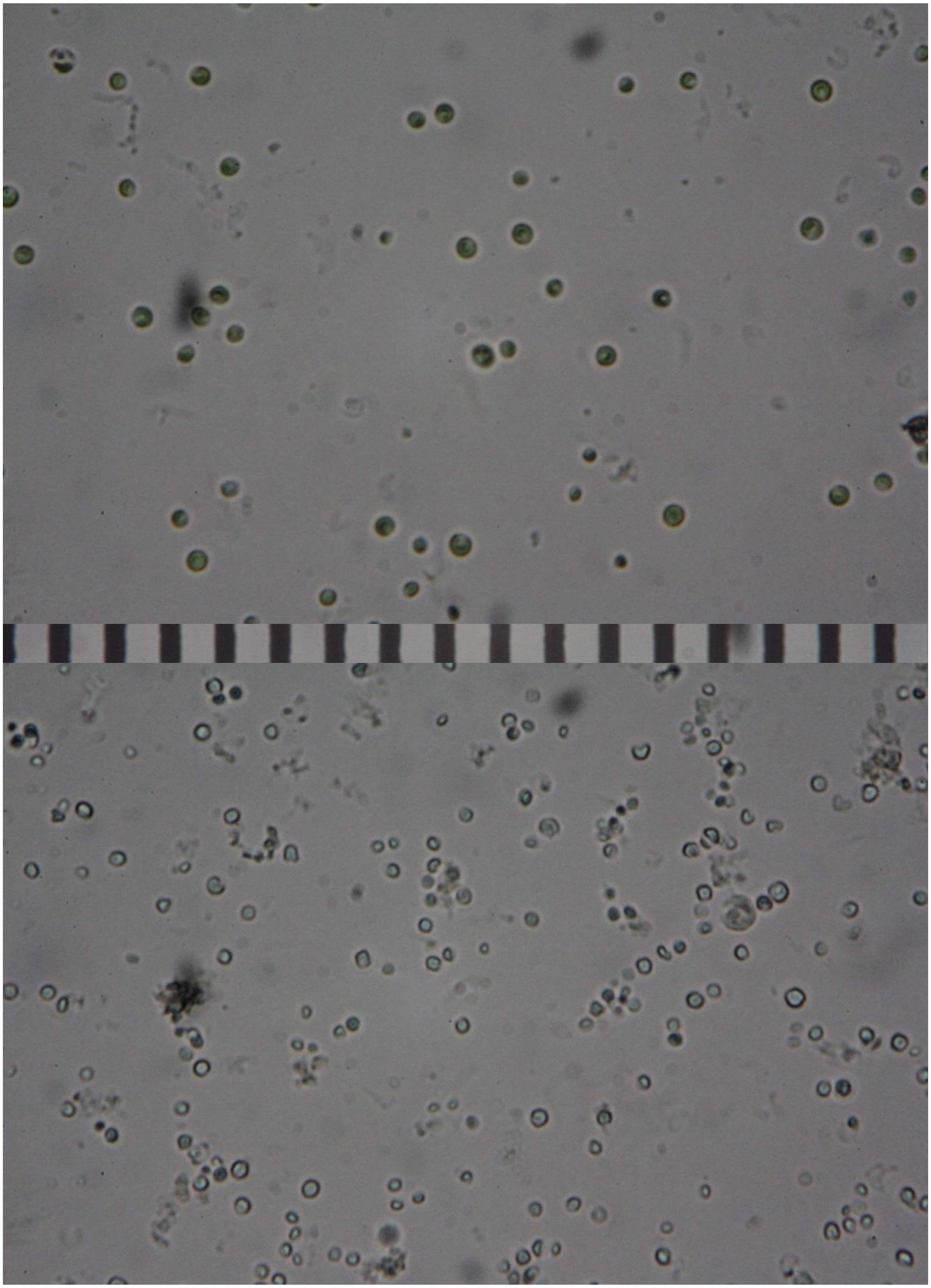

Figure 30. Microscope Images of Untreated Algae and 6 V, 20%, 100 Hz Treated Algae. Top picture is untreated algae, bottom picture is a 5 minute batch run: 6 V, 20%, 100 Hz remixed. 1 division on scale is 10 μm

Figure 29 clearly shows that the 3 V DC treated algae cells are not as green as the untreated culture indicating that chlorophyll has been oxidized and that the cell wall has been compromised. The algae cells subjected to 6 V, 20%, 100 Hz are also noticeably smaller in diameter than the untreated algae cells and many have a collapsed or deformed appearance (Figure 30). The smaller diameter and crumpled shape could indicate two events occurring. Under certain electrolysis conditions, the cells could be dehydrated with only water leaving the cell, or cell lysis may be occurring and releasing cellular contents into the media.

There was some difficulty remixing the foam generated from the 6 V, 20%, 100 Hz experiment back into the bulk fraction. The bubbles at the surface were simply difficult to pop. After a few minutes of stirring, some foam reduction was achieved but a moderate amount still remained at the surface. Algae cells remaining in the foam would not be represented in the pictures.

Due to the dramatic changes in the absorbance spectra and optical characteristics of the treated algae, we had to modify our approach to determine fractionation efficiency. With the custom real-time harvest efficiency monitoring device, it would not be possible to attribute the degree to which changes in optical properties in culture were due to biomass recovery/ flotation, or to disruption of cells and cellular pigments. The revised approach to resolve this issue was to conduct algae separation experiments in batch runs and measure absorbance of the top and lower fractions after the runs with a commercial spectrophotometer. This procedure is described in sections 5.7.3 and 5.7.4 of this report. The effect of algae bleaching is assumed to be the equivalent in all sections of the electrolysis vessel, and therefore that the relative optical densities in these fractions provides a reasonable approximation of the relative biomass contents of these fractions.

6.4.4. Biomass Separation Results

Percent recovery of biomass from suspension was less than 10% for all treatments (Figure 31). The treatment with the highest percent recovery of biomass was found at 6 V, 20%, 25 Hz and yielded an average recovery of 6.8%.

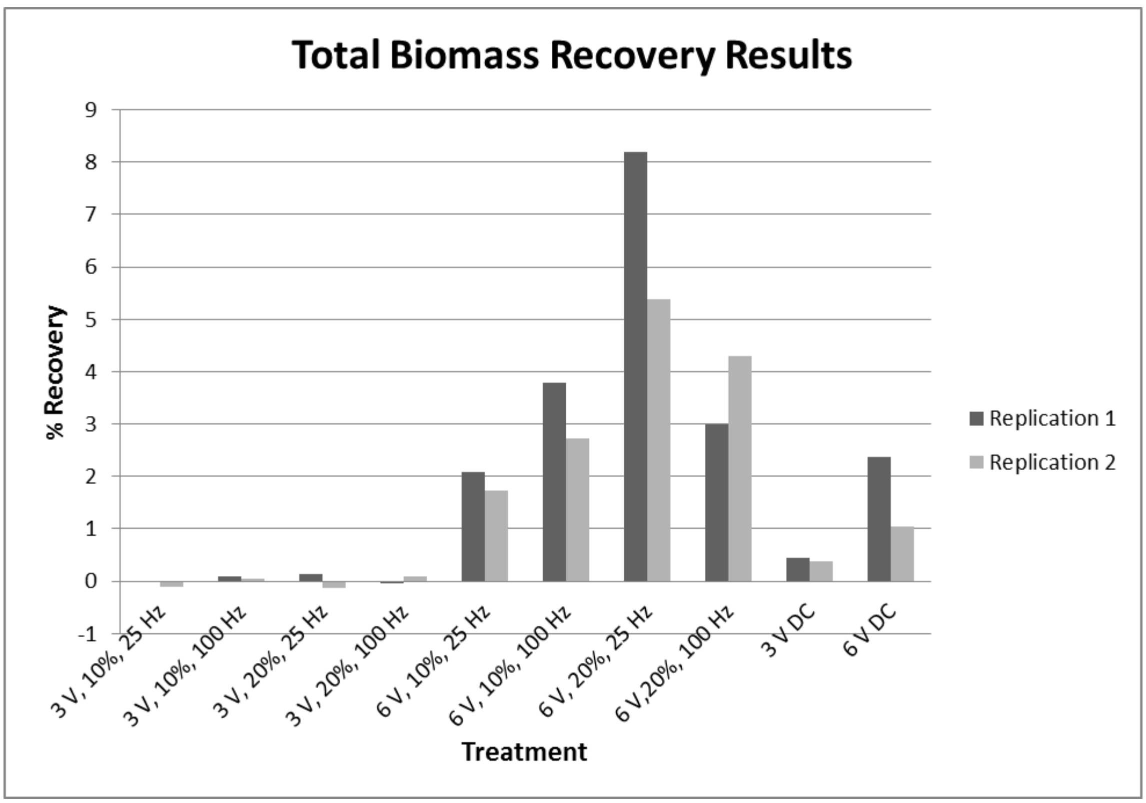

Figure 31. Biomass Recovery Results

The 6.8% biomass recovery corresponded to 521.5 KJ g^{-1} dry material recovered. This value was calculated based on the original biomass contents of the cultures inferred from photometric measurements and the energy used for each replicate. The 3 V pulsed runs show virtually no separation at all, illustrating that operating at close to optimal thermodynamic efficiency for gas generation is clearly not practical for indusrun scale separation. The volume of gas and quantity of bubbles was not significant enough to remove algae from suspension.

In a study by Dassey and Theegala (2013), the required energy corresponding to 17% algae removal would be 169.4 KJ g^{-1} dry material recovered. The electroflotation energy input for the highest biomass recovery in our experiments (6.8% recovery corresponding to 521.5 KJ g^{-1}) was over three times higher than the centrifugation separation discussed above. For a perfect energy comparison of the two different methods, the same concentration would have to be used in both. The initial algae culture concentration in the Dassey and Theegala (2013) study was 100 mg dry biomass L^{-1}. The average algae concentration in our experiments, inferred from optical measurements, was 61.4 mg dry biomass L^{-1} for the electroflotation treatment. Higher recovered mass may have occurred if the concentration was 100 mg dry biomass L^{-1}. This would have reduced the difference in energy input per recovered biomass between the compared electroflotation and centrifugation tests.

One possible reason for the low percent recoveries found during electroflotation may be the small size of the algae. The *Chlorella* sp. cultures used in this research were composed of fine, unicellular particles (diameter of 2 µm-5 µm; Figures 29 and 30). As previously mentioned, fine particles are more difficult to isolate from suspension in a flotation process.

An interesting observation from Figure 31 is that the 6 V DC treatment had a lower % recovery than the 6 V pulsed treatments. This can be attributed to the poor foam formation during the 6 V DC treatments. The 6 V DC treatments had extremely vigorous electrolysis with high rates of gas generation that created rapid mixing and also formed large bubbles at the surface that were prone to popping. The 6 V pulsed runs had less vigorous electrolysis and the foam formed was composed of smaller bubbles that were more stable at the surface (Figure 32).

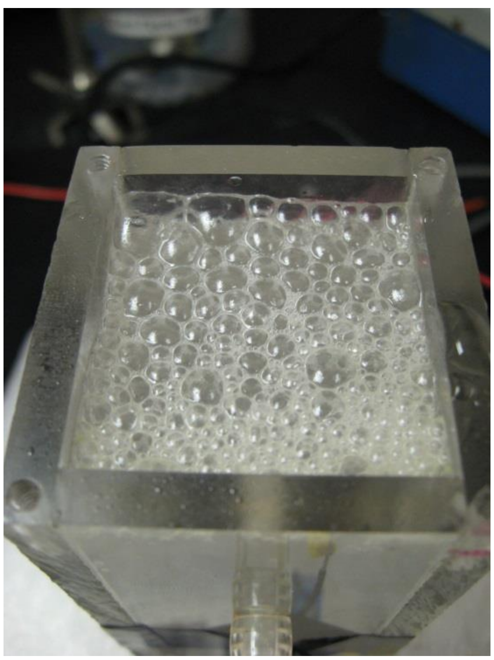

1st Replication: 6 V, 20%, 25 Hz End of Run

1st Replication: 6 V DC End of Run

Figure 32. Foam Formation Comparisons. 6 V, 20%, 25 Hz vs. 6 V DC runs.

Foam stability is critical because it traps the algae at the surface and keeps it from reentering into the bulk suspension. Use of a surfactant to stabilize the foam may improve biomass recovery from electroflotation, but generally the use of additives is regarded as undesirable based on the added expense and potential contamination of downstream processes.

The ANOVA indicates that duty cycle is a significant factor at the 0.05 significance level, applied potential is significant at the 0.05 significance level, the interaction between duty cycle and applied potential is significant at the 0.05 significance level, the interaction between frequency and duty cycle were significant at the 0.05 significance level, and that the interaction between frequency, duty cycle, and applied potential is significant at the 0.05 significance level (Table 7).

Table 7. Biomass Recovery ANOVA. Green highlights significant factors and interactions

Source	df	SS	MS	F	F (0.05)
Total	15	91.39			
Treatment	(7)				
A (Frequency)	1	0.68	0.68	0.98	5.32
B (Duty Cycle)	1	6.96	6.96	10.13	5.32
C (Applied Potential)	1	60.35	60.35	87.78	5.32
AxB	1	5.30	5.30	7.70	5.32
AxC	1	0.94	0.94	1.36	5.32
BxC	1	6.87	6.87	9.99	5.32
AxBxC	1	4.80	4.80	6.98	5.32
Error	8	5.50	0.69		

With duty cycle and applied potential both being significant main factors, the separation of algae appears to be most dependent on the volume of gas being generated. Higher duty cycles and applied potentials generally yielded higher gas generation that typically led to higher rates of biomass recovery.

6.5. Lipid Separation Results

It was decided to evaluate lipid fractions after observing the disruption of cells to determine if lipids remained with the cellular debris or if they partitioned off on their own. If lipids were released from the cells, it was hypothesized that they would likely float to the surface because they have a lower density than the media.

Separation of lipids from suspension was generally more effective at the higher applied potentials (Figure 33), mirroring results of the biomass recovery.

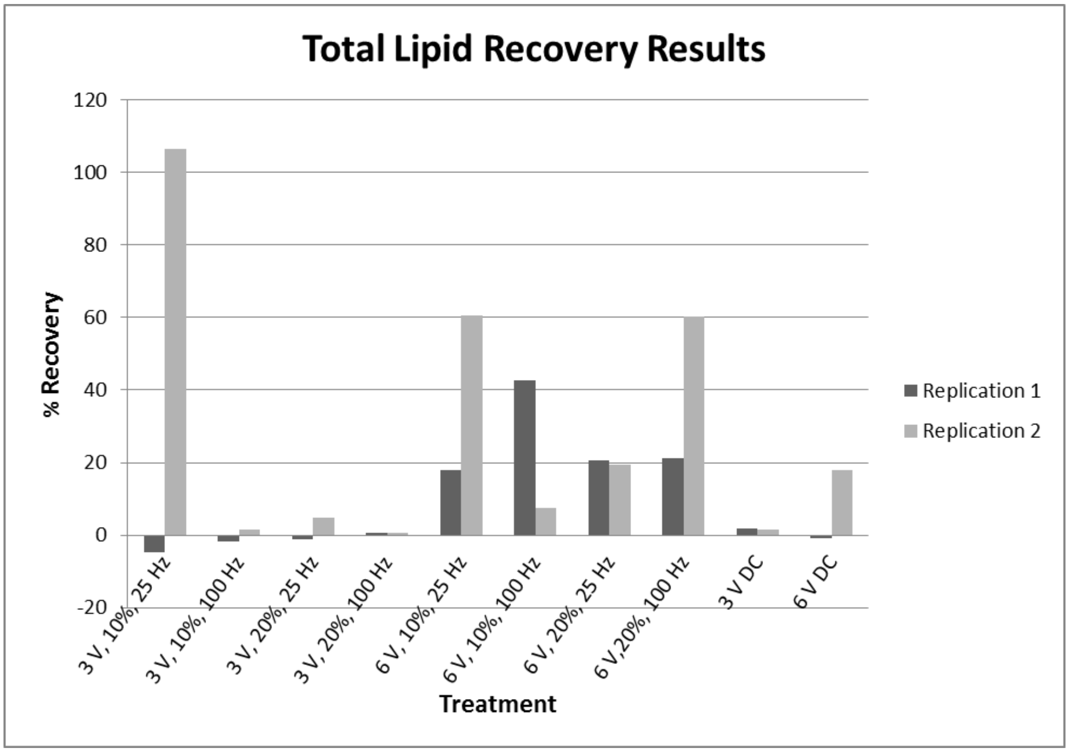

Figure 33. Total Lipid Recovery Results

This is to be expected because the lipids are of course contained within the algae cells. Even when cell lysis occurs, it has been reported that the lipids tend to stay with the cell debris in aqueous environments (Gerde et al., 2012) so they would likely aggregate with other biomass components.

Large variability generally existed between runs of the same treatment (Figure 33). Furthermore, the measured fluorescence values from the Nile red stained samples were highly variable not just for different replicates of the same treatments, but also for duplicate aliquots of the same samples (Appendices 3 and 4). It appears that there is high variability inherent to the lipid analysis procedure that was followed. The wavelength at which peak fluorescence occurred was not the same for all runs

(Appendices 3 and 4). The reason for this is still unknown. There may be an interaction between the Nile red, hypochlorite, and lipids, or it may be our analysis methods. Another potential cause of variability in fluorescence measurements may be due to the occasional use of ethanol to rinse/clean the cuvette. A single rinse of water was used following the application of ethanol to remove remnants, but it may be possible that trace amounts of ethanol remained in the cuvette. Nile red will fluoresce in ethanol approximately 20x more than in water (Greenspan and Fowler, 1985) so even small amounts of ethanol present would falsely increase fluorescence. The wavelength of peak fluorescence of Nile red in ethanol is approximately 629 nm (Greenspan and Fowler, 1985) and could have shifted spectra measurements as well. Variability in all samples and the media backgrounds may have resulted from not completely removing all traces of ethanol during the water rinse. Sample backgrounds accounting for the intrinsic fluorescence of the samples may have been effected by the presence of ethanol as well but is likely much less significant than samples treated with Nile red.

The conditions resulting in the highest lipid recovery, excluding the 3 V, 10%, 25 Hz treatment which is assumed to be an error, were 6 V, 20%, 100 Hz with an average of 40.8% lipid recovery. This provides further evidence of cell lysis and disgorgement of cellular contents during these experiments because the lipid fraction recovery is so much higher than the 3.6% recovery of the biomass fraction observed for the same experimental treatment conditions. Although lipids tend to aggregate with cell debris, some lipids may be being released into the bulk leading to higher observed lipid separations. Lipids are buoyant and would have a greater tendency to float to the surface. This is one possible explanation for why the lipid separation was so much higher than the biomass separation. Optimization of the lipid analysis procedure is recommended before drawing firm conclusions. From an energy standpoint, the 40.8% lipid recovery corresponds to a recovery of 11.3% of electrical energy expended for electroflotation as a liquid fuel, assuming that 30% of the dry algal biomass is lipids, using the estimated algae content of the cultures from optical measurements, the energy inputs for the 6 V, 20%, 100 Hz runs, and using the lower heating value for biodiesel combustion (37.25 MJ kg^{-1}) (Lapuerta et al., 2008) as the value for burning lipids.

No significant factors were identified by the ANOVA because the variability in the results was too high (Table 8).

Table 8. Lipid Recovery ANOVA

Source	df	SS	MS	F	F (0.05)
Total	15	14210.87			
Treatment	(7)				
A (Frequency)	1	521.13	521.13	0.49	5.32
B (Duty Cycle)	1	672.87	672.87	0.63	5.32
C (Applied Potential)	1	1290.14	1290.14	1.21	5.32
AxB	1	1801.93	1801.93	1.69	5.32
AxC	1	858.74	858.74	0.81	5.32
BxC	1	501.33	501.33	0.47	5.32
AxBxC	1	53.48	53.48	0.05	5.32
Error	8	8511.24	1063.90		

7. Conclusions

Design, fabrication, and operation of a benchtop scale electroflotation assembly were successfully executed. Using the assembly, experiments in a 2^3 factorial experimental design were performed. The experiments investigated the effects that the applied potential, frequency, and duty cycle had on bubble size distributions, gas generation efficiency, and total biomass and lipid fraction recoveries from *Chlorella* sp. cultured in a marine media.

The 3 V treatments produced mean bubble sizes smaller than the 6 V treatments. A higher applied potential caused higher current densities which may have led to a higher degree of gas supersaturation and the generation of larger bubble sizes. Current pulsing was conducive to evolving smaller bubbles during the electrolysis process in 3 V treatments and provided greater distribution uniformity in 6 V treatments by reducing the number of large outlier bubbles. Applied potential was the only significant factor affecting bubble size determined from the ANOVA. Decreasing the applied potential reduced the mean bubble size. The conditions resulting in the presumably most favorable (smallest) bubble sizes were 3 V, 20%, 25 Hz with an average of 30.1 µm bubble mean diameter. The smallest median bubble diameter (25.0 µm) occurred at 3 V, 10%, 25 Hz.

Gas generation efficiency is highly dependent on frequency. For 3 V pulsed, treatments increasing the frequency from 25 Hz to 100 Hz resulted in an increase in gas generation efficiency while for 6 V treatments the opposite was true. The treatment with the highest gas generation efficiency was 3 V DC at 1.69×10^{-6} (mol J^{-1}). This suggests that, especially under conditions where electrolysis is more kinetically limited, current pulsing may lead to larger fractions of dissolved gas diffusing into the bulk solution rather than supporting bubble nucleation and growth. From the ANOVA, frequency and applied potential were significant factors for gas generation efficiency, and there was a significant interaction between frequency and applied potential.

Design, fabrication, and calibration of a real-time microalgae harvesting monitoring device was performed. The device sensitivity was about 5x less than that of a commercial spectrophotometer. Other lab members are currently evaluating a revised design to address some observed limitations in the device sensitivity. The device was not used in runs due to the bias that algae bleaching (a result of the marine electrolysis process generating reactive chlorine compounds) would have introduced on the measurements. This device might be useful in evaluating electroflotation of algae or other particles from a chloride-free media. It may also find utility in monitoring electroflotation of non-biological solids from a marine environment.

Electrolysis in a marine environment produces hypochlorite. This bleached the algae and at high applied potentials may have even lysed the algae. Hypochlorite is a strong oxidizer and may destroy many of the algae constituents. This electroflotation in a marine environment may not suitable for harvesting microalgae for nutraceuticals. Although the Nile red analysis was somewhat inconclusive, it may suggest that quantities of the lipids could be recovered by short electroflotation treatments and a single step lipid recovery may be possible. The generation of hypochlorite may also find use in areas where separation, disinfection, and cell death are desired. For example, if an algae farm wanted to remove an undesirable algae, they could use marine electrolysis to separate and kill the unwanted algae in a single step. One such situation might arise in spirulina culture, which uses large rotary screens to separate out the spirulina with relatively large filaments. This process results in natural selection for spirulina with smaller filaments which are harder to isolate. The Spirulina farm might be interested in "sterilizing" or recovering these smaller spirulina from the treated stream.

Percent recovery of biomass was generally very low (less than 10%) most likely due to the small size of the algae and poor foam formation. The most effective treatment for biomass recovery was 6 V, 20%, 25 Hz with an average of 6.8% recovery corresponding to 521.5 KJ g^{-1} biomass recovered. The pulsed 3 V treatments did not result in substantial biomass recovery because the volume of gas generated and the quantity of bubbles were not sufficient to provide separation. Duty cycle and applied potential were significant factors from the ANOVA and increasing both factors typically resulted in improved biomass recovery. Frequency and duty cycle interaction, duty cycle and applied potential interaction, and the 3 way interaction of all factors were all also found to be significant from the ANOVA.

The 6 V treatments resulted in greater separation of lipids than the 3 V runs (excluding the 3 V, 10%, 25Hz treatment assumed to be an error). The lipid percent recoveries were nearly always higher than the percent recoveries of biomass material. This may be an indicator that cell lysis is occurring during the electrolysis process and lipids are being disgorged from the cells. Lipids are more buoyant and would more readily float to the top. The treatment with the highest lipid recovery was 6 V, 20%, 100

Hz, with an average of 40.8% lipid recovery corresponding to a recovery of 11.3% of electrical energy expended for electroflotation as a liquid fuel. The results for the lipid analysis were highly variable and somewhat inconclusive. It is worth consideration before coming to any firm conclusions from this analysis. Due to the high variability, no significant effects were found from the lipid analysis ANOVA.

8. References

Bui, D., and P. C. Hauser. 2013. Absorbance measurements with light-emitting diodes as sources: Silicon photodiodes or light-emitting diodes as detectors? *Talanta* 116: 1073–1078.

Balaji, R., B. S. Kannan, J. Lakshmi, N. Senthil, S. Vasudevan, G. Sozhan, A. K. Shukla, and S. Ravichandran. 2009. An alternative approach to selective sea water oxidation for hydrogen production. *Electrochemistry Communications* 11: 1700–1702.

Belmont, C., R. Ferrigno, O. Leclerc, and H. H. Girault. 1998. Coplanar interdigitated band electrodes for electrosynthesis. Part 4: Application to sea water electrolysis. *Electrochimica Acta 44*: 597-603.

Bertozzini, E., L. Galluzzi, A. Penna, and M. Magnani. 2011. Application of the standard addition method for the absolute quantification of neutral lipids in microalgae using Nile red. *Journal of Microbiological Methods* 87: 17–23.

Bishop, W. M., and H. M. Zubeck. 2012. Evaluation of microalgae for use as nutraceuticals and nutritional supplements. *Journal of Nutrition & Food Sciences* 2:5.

Box, G. E. P., J. S. Hunter, W. G. Hunter. 2005. Statistics for Experimenters. 2nd Edition. John Wiley & Sons, Inc., Hoboken , NJ.: 173-222.

Chandrasekar, M. S., and M. Pushpavanam. 2008. Pulse and pulse reverse plating—Conceptual, advantages and applications. *Electrochimica Acta* 53: 3313–3322.

Chisti, Y., 2007. Biodiesel from microalgae. *Biotechnology Advances* 25: 294–306.

Christenson, L., R. Sims. 2011. Production and harvesting of microalgae for wastewater treatment, biofuels, and bioproducts. *Biotechnology Advances* 29: 686-702.

Csordas, A., and J.Wang. 2004. An integrated photobioreactor and foam fractionation unit for the growth and harvest of Chaetoceros spp. in open systems. *Aquacultural Engineering* 30: 15–30.

Dassey, A. J., and C. S. Theegala. 2013. Harvesting economics and strategies using centrifugation for cost effective separation of microalgae cells for biodiesel applications. *Bioresource Technology* 128: 241-245.

Dehaeck S., J. P. A. J. van Beeck. 2008. Multifrequency interferometric particle imaging for gas bubble sizing. *Exp Fluids* 45: 823-831

Didenkulov, I. N., A. M. Sutin, and S. W. Yoon. 2000. The difference frequency technique for bubble size and Doppler velocity measurements. American Institute of Physics Conference Proceedings.

Fathollahi, F., M. Javanbakht, P. Norouzi, and M. R. Ganjali. 2011. Comparison of morphology, stability and electrocatalytic properties of $Ru_{0.3}Ti_{0.7}O_2$ and $Ru_{0.3}Ti_{0.4}Ir_{0.3}O_2$ coated titanium anodes. *Russian Journal of Electrochemistry* 47:11, 1281–1286.

Feng, G., F. Zhang, L. Cheng, X. Xu, L. Zhang, and H. Chen. 2013. Evaluation of FT-IR and Nile Red methods for microalgal lipid characterization and biomass composition determination. *Bioresource Technology* 128: 107–112.

Gao, S., M. Du, J. Tian, J. Yang, J. Yang, F. Ma, and J. Nan. 2010. Effects of chloride ions on electro-coagulation-flotation process with aluminum electrodes for algae removal. *Journal of Hazardous Materials* 182: 827–834.

Gerde, J. A., M. Montalbo-Lomboy, L. Yao, D. Grewell, and T. Wang. 2012. Evaluation of microalgae cell disruption by ultrasonic treatment. *Bioresource Technology* 125: 175–181.

Greenspan, P., and S. D. Fowler. 1985. Spectrofluorometric studies of the lipid probe, nile red. *Journal of Lipid Research* 26: 781-789

Griffiths, M. J., R. G. Dicks, C. Richardson, and S. T. L. Harrison. 2011. Advantages and challenges of microalgae as a source of oil for biodiesel.

Henderson, R. K., S. A. Parsons, and B. Jefferson. 2008. Surfactants as bubble surface modifiers in the flotation of algae: Dissolved air flotation that utilizes a chemically modified bubble surface. *Environmental Science & Technology* 42: 4883–4888.

Khosla, N. K., S. Venkatachalam, and P. Somasundaran. 1991. Pulsed electrogeneration of bubbles for electroflotation. *Journal of Applied Electrochemistry* 21: 986–990.

Koretsky, M. D. 2004. Engineering and Chemical Thermodynamics. John Wiley & Sons, Inc., Hoboken, NJ.: 215.

Lam, M., and K. Lee. 2012. Microalgae biofuels: A critical review of issues, problems and the way forward. *Biotechnology Advances* 30: 673–690.

Lapuerta, M., O. Armas, and J. Rodriguez-Fernandez. 2008. Effect of biodiesel fuels on diesel engine emissions. *Progress in Energy and Combustion Science* 34: 198–223.

Miettinen, T., J. Ralston, and D. Fornasiero. 2010. The limits of fine particle flotation. *Minerals Engineering* 23: 420-437.

Nagai, N., M.Takeuchi, T. Kimura, and T. Oka. 2003. Existence of optimum space between electrodes on hydrogen production by water electrolysis. *International Journal of Hydrogen Energy* 28: 35–41.

Pearsall, R. V., R. L. Connelly, M. E. Fountain, C. S. Hearn, M. D. Werst, R. E. Hebner, and E. F. Kelley. 2011. Electrically dewatering microalgae. *IEEE Transactions on Dielectrics and Electrical Insulation* 18:5 1578–1583.

Sanyano, N., P. Chetpattananondh, and S. Chongkhong. 2013. Coagulation – flocculation of marine Chlorella sp . for biodiesel production. *Bioresource Technology* 147: 471–476.

Sarkar, Md. S. K. A., G. M. Evans, and S. W. Donne. 2010. Bubble size measurement in electroflotation. *Minerals Engineering* 23: 1058–1065.

Sarkar, M. S. K. A., S. W. Donne, and G. M. Evans. 2011. Utilization of hydrogen in electroflotation of silica. *Advanced Powder Technology* 22: 482–492.

Uduman, N., Y. Qi, M. K. Danquah, G. M. Forde, and A. Hoadley. 2010. Dewatering of microalgal cultures: A major bottleneck to algae-based fuels. *Journal of Renewable and Sustainable Energy* 2: 012701.

US EPA. 2013. Renewable Fuel Standard (RFS). http://www.epa.gov/OTAQ/fuels/renewablefuels/

Zhang, W., S. J. Spencer, P. Coghill. 2012. An acoustic technique for measurement of bubble solids mass loading- (a) Fundamental study of single bubble. *Minerals Engineering* 36-38: 45-52.

Zhou, M., L. Liu, Y. Jiao, Q. Wang, and Q. Tan. 2011. Treatment of high-salinity reverse osmosis concentrate by electrochemical oxidation on BDD and DSA electrodes. *Desalination* 277: 201-206.

9. Appendices

Appendix 1.

SEM Images of DSA Electrode

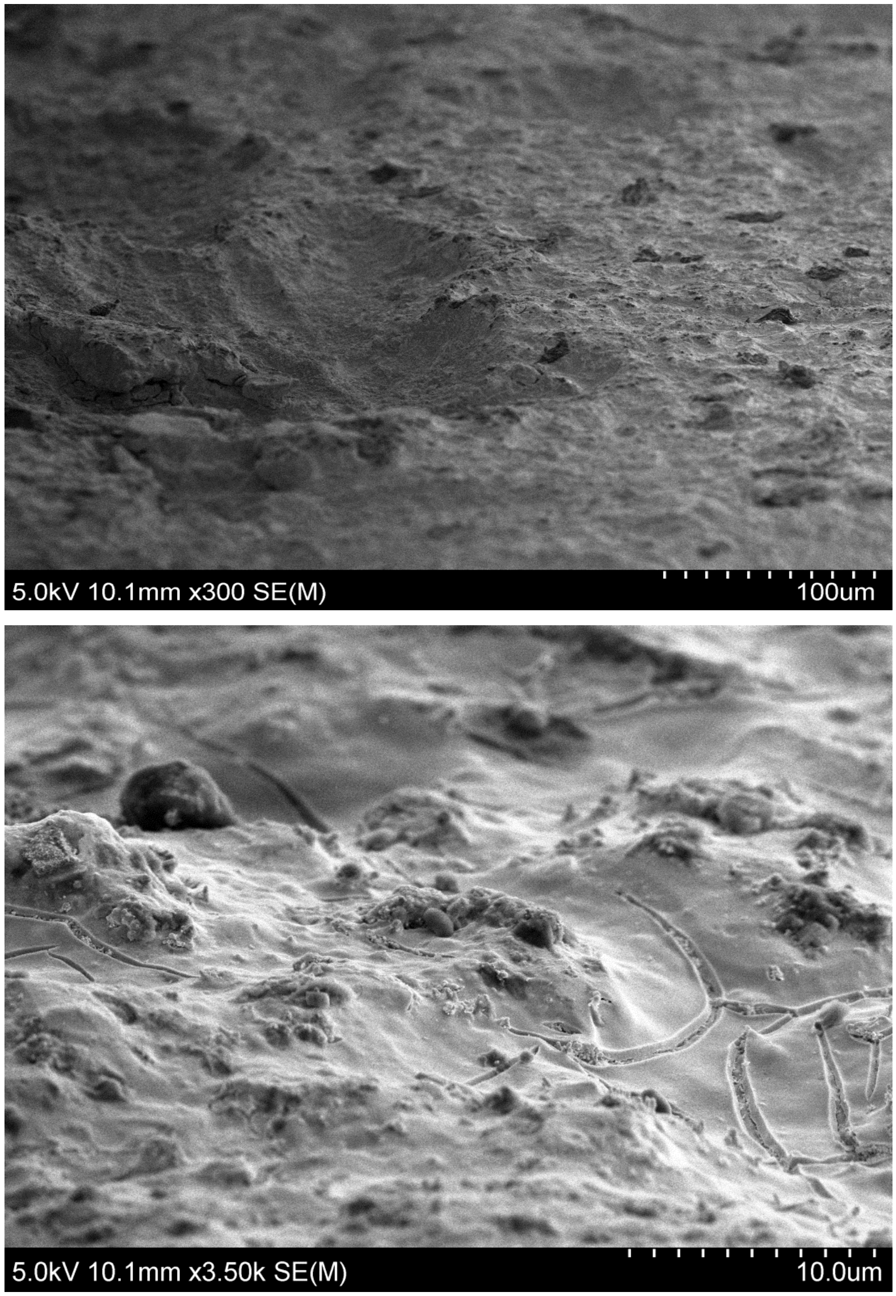

Figure A1. MMO Coating. Coating has a "cracked" mud surface morphology. All ten divisions make up the scale value found in the lower right corner. E.g. 10 μm, each division: 1 μm

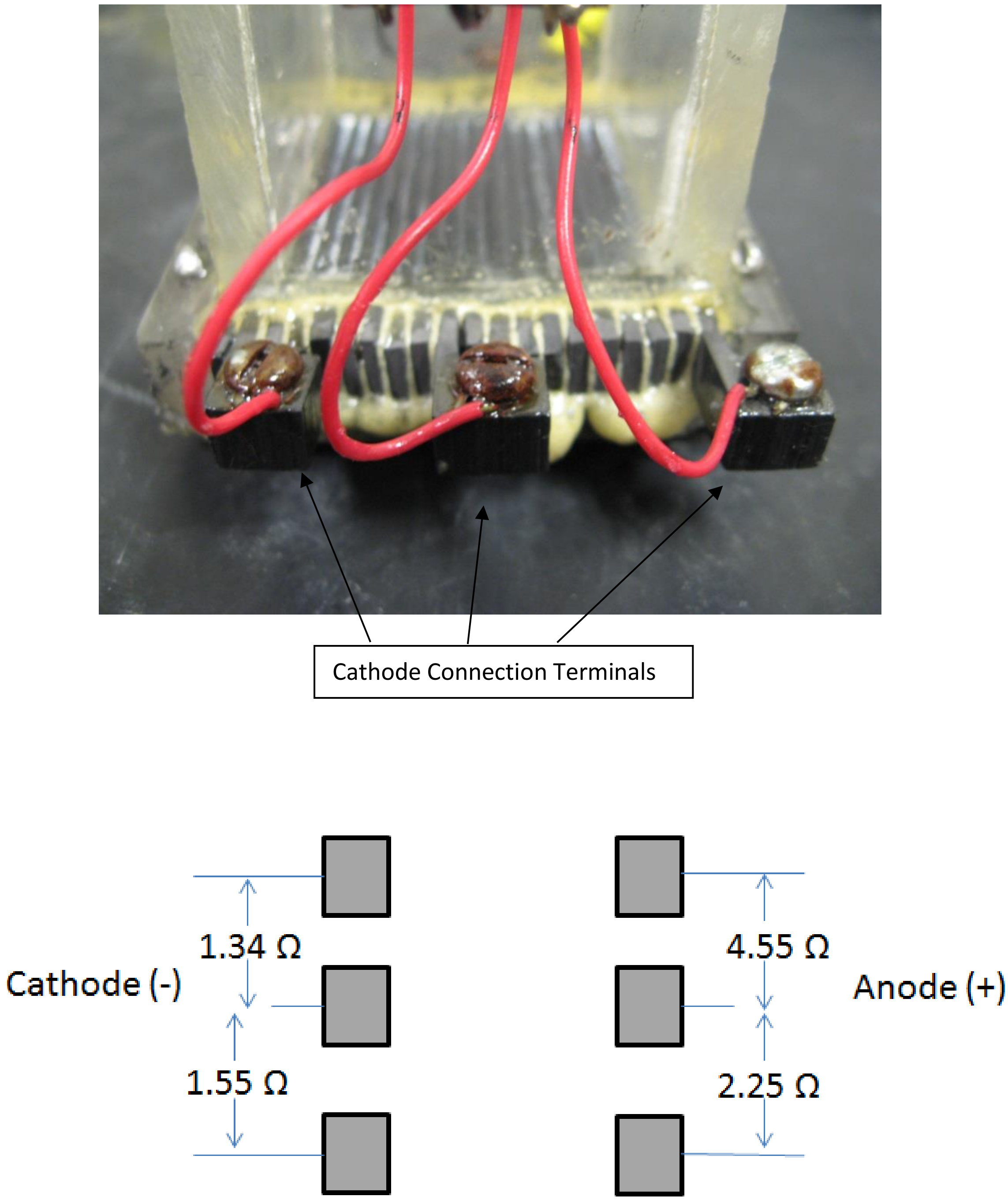

Figure A2. Wire Connection Terminal Picture and Connectivities. Connectivites are the resistances between the terminals generated by imperfect graphite interconnects.

Appendix 3.

Table A1. 1st Replication Lipid Separation Data and Results

				Average								Average					
	Aliquot	**Peak RFU**	**λ_{max}**	**Peak RFU**	**λ_{max}**	**back.**	**media**	**T-back.-media**	**Aliquot**	**Peak RFU**	**λ_{max}**	**Peak RFU**	**λ_{max}**	**back.**	**media**	**B-back.-media**	**% recovery**
3 V, 10%, 25 Hz	**T1,1**	81.44	647.50	97.12	647.50	7.30	90.41	-0.59	**B1,1**	100.90	648.00	98.11	646.75	6.13	89.67	2.31	**-4.79**
	T1,2	112.80	647.50						**B1,2**	95.31	645.50						
6 V, 20%, 100 Hz	**T2,1**	327.70	616.50	335.90	617.75	17.48	74.81	243.61	**B2,1**	103.00	608.00	110.10	611.25	6.68	74.50	28.92	**21.26**
	T2,2	344.10	619.00						**B2,2**	117.20	614.50						
3 V, 20%, 25 Hz	**T3,1**	110.50	610.00	112.95	609.00	20.14	74.43	18.38	**B3,1**	116.00	613.00	118.25	611.75	15.76	74.18	28.31	**-1.29**
	T3,2	115.40	608.00						**B3,2**	120.50	610.50						
3 V, 10%, 100 Hz	**T4,1**	129.10	609.00	127.40	608.50	16.16	74.43	36.81	**B4,1**	171.10	646.00	158.20	626.75	13.84	77.86	66.50	**-1.65**
	T4,2	125.70	608.00						**B4,2**	145.30	607.50						
3 V DC	**T5,1**	297.50	621.50	286.50	623.25	12.60	76.03	197.87	**B5,1**	225.60	622.50	218.95	623.50	10.17	76.37	132.41	**1.77**
	T5,2	275.50	625.00						**B5,2**	212.30	624.50						
6 V, 10%, 25 Hz	**T6,1**	342.80	621.00	337.85	621.75	20.40	75.28	242.17	**B6,1**	137.10	603.50	126.05	602.00	17.93	73.82	34.30	**18.06**
	T6,2	332.90	622.50						**B6,2**	115.00	600.50						
6 V, 10%, 100 Hz	**T7,1**	680.40	621.50	636.50	622.25	25.74	75.28	535.48	**B7,1**	106.80	592.50	111.15	593.75	14.69	71.44	25.02	**42.59**
	T7,2	592.60	623.00						**B7,2**	115.50	595.00						
6 V DC	**T8,1**	168.40	594.50	166.35	594.50	20.05	71.78	74.52	**B8,1**	173.30	613.50	179.50	612.00	7.55	74.18	97.78	**-0.87**
	T8,2	164.30	594.50						**B8,2**	185.70	610.50						
6 V, 20%, 25 Hz	**T9,1**	521.20	617.50	540.85	617.50	28.78	74.81	437.26	**B9,1**	124.90	608.50	136.30	611.50	8.34	74.18	53.79	**20.59**
	T9,2	560.50	617.50						**B9,2**	147.70	614.50						
3 V, 20%, 100 Hz	**T10,1**	227.40	621.50	228.50	621.25	11.86	75.59	141.05	**B10,1**	208.40	635.50	209.80	631.25	10.12	79.82	119.86	**0.64**
	T10,2	229.60	621.00						**B10,2**	211.20	627.00						

*Peak fluorescence emission relative units (Peak RFU)
Wavelength at peak fluorescence emission (λ_{max})
Top and bottom aliquot of run (T and B). e.g. T1,2 is the 2nd replicate aliquot of the top fraction from the first run
Background of algae sample with no Nile Red at the average λ_{max} (back.)
Background of media stained with Nile red at average λ_{max} (media)

Appendix 4.

Table A2. 2nd Replication Lipid Separation Data and Results

				Average								Average					
	Aliquot	**Peak RFU**	**λ_{max}**	**Peak RFU**	**λ_{max}**	**back.**	**media**	**T-back.-media**	**Aliquot**	**Peak RFU**	**λ_{max}**	**Peak RFU**	**λ_{max}**	**back.**	**media**	**B-back.-media**	**% recovery**
6 V, 10%, 100 Hz	**T1,1**	665.00	619.50	654.30	618.75	17.43	74.98	561.89	**B1,1**	237.70	621.50	261.30	620.75	10.18	75.59	175.53	**7.41**
	T1,2	643.60	618.00						**B1,2**	284.90	620.00						
3 V DC	**T2,1**	457.10	622.00	433.75	620.50	22.84	75.59	335.32	**B2,1**	327.80	619.50	316.55	622.25	11.84	75.28	229.43	**1.65**
	T2,2	410.40	619.00						**B2,2**	305.30	625.00						
3 V, 10%, 25 Hz	**T3,1**	137.30	650.00	128.70	647.50	6.88	90.41	31.40	**B3,1**	81.04	642.00	95.92	644.25	6.90	89.09	-0.07	**106.55**
	T3,2	120.10	645.00						**B3,2**	110.80	646.50						
6 V, 20%, 25 Hz	**T4,1**	658.90	620.50	663.20	622.00	23.00	75.28	564.92	**B4,1**	181.70	605.50	158.35	607.25	10.01	74.16	74.18	**19.39**
	T4,2	667.50	623.50						**B4,2**	135.00	609.00						
3 V, 20%, 100 Hz	**T5,1**	148.20	626.00	152.85	625.25	9.26	76.77	66.81	**B5,1**	147.70	636.00	145.60	631.75	8.08	80.94	56.59	**0.65**
	T5,2	157.50	624.50						**B5,2**	143.50	627.50						
3 V, 20%, 25 Hz	**T6,1**	178.10	617.00	169.25	626.00	8.70	77.28	83.27	**B6,1**	111.90	622.00	124.20	634.50	6.48	83.50	34.22	**4.95**
	T6,2	160.40	635.00						**B6,2**	136.50	647.00						
6 V, 20%, 100 Hz	**T7,1**	378.10	618.00	379.75	618.50	11.97	74.98	292.80	**B7,1**	88.81	609.00	87.74	610.00	6.34	74.56	6.84	**60.33**
	T7,2	381.40	619.00						**B7,2**	86.66	611.00						
6 V, 10%, 25 Hz	**T8,1**	274.70	622.00	274.55	621.50	12.85	75.28	186.42	**B8,1**	85.57	601.50	86.99	602.75	8.96	73.72	4.30	**60.61**
	T8,2	274.40	621.00						**B8,2**	88.40	604.00						
6 V DC	**T9,1**	156.40	598.00	160.40	599.50	10.80	73.43	76.17	**B9,1**	93.70	611.00	91.20	610.75	5.89	74.50	10.81	**18.03**
	T9,2	164.40	601.00						**B9,2**	88.69	610.50						
3 V, 10%, 100 Hz	**T10,1**	115.70	649.00	114.10	648.75	6.34	90.43	17.34	**B10,1**	102.40	646.50	107.65	647.25	5.79	89.67	12.20	**1.51**
	T10,2	112.50	648.50						**B10,2**	112.90	648.00						

*Peak fluorescence emission relative units (Peak RFU)
Wavelength at peak fluorescence emission (λ_{max})
Top and bottom aliquot of run (T and B). e.g. T1,2 is the 2nd replicate aliquot of the top fraction from the first run
Background of algae sample with no Nile Red at the average λ_{max} (back.)
Background of media stained with Nile red at average λ_{max} (media)